NIGHTTIME IDENTIFICATION OF F REGION CURRENTS FROM CHAMP SATELLITE OBSERVATIONS OVER EQUATORIAL AFRICA

By

AWUOR OCHIENG ADERO

Dissertation submitted in partial fulfillment for the degree of Master of Science of the University of Nairobi

JUNE, 2011.

DECLARATION

This dissertation is my own work and has not been examined or submitted for examination in any other university.

Awuor, Ochieng Adero

I56/78046/2009

Signature..... Date..08/07/2011.....

This dissertation has been submitted for examination with the approval of my supervisors.

Prof. Paul Baki

Department of Technical and Applied Physics

Kenya Polytechnic University College

P.O Box 52428, 00200 Nairobi

Signature..... Date..12/7/2011.....

and

Dr. C. Mito

Department of Physics

University of Nairobi

P.O Box 30197, 00100 Nairobi

Signature..... Date..08/07/2011.....

Abstract

This dissertation investigates the ionospheric F-region currents inferred from the interpretation of the magnetic signatures using Challenging Minisatellite Payload (CHAMP) satellite data. The observations are limited to the quiet days, with the Dst index less than 20 and on the nightside of 2000hrs to 0500hrs for a period Jan, 2001 to Dec, 2001. In this study, we report for the first time, the F-region currents as inferred from the CHAMP vector data. We find the spatial confinement of the currents to the near the equatorial region bounded by the Appleton anomaly and their appearance in the pre-midnight and post-midnight sectors. The current densities are greatly varied along all the three magnetic field components with the z-component recording the highest values. The current densities along y-component is highest in the months of November, about 7.7 mA/m, but generally less than 5.6 mA/m for the rest of the months. The months of September, August and November record the highest current densities with August recording a density of 31.35mA/m along the x-component showing the seasonal variation of the currents along all the three magnetic field components.

ACKNOWLEDGEMENT

Firstly, I would like to express my special thanks to my supervisor, Prof Paul Baki, for his encouragement of this research, and for inspiring and supporting my interest in the field of Ionospheric Physics and his co-supervisor Dr. C.O Mito for his invaluable advise. My heart-felt appreciation goes also to both the Hermanus Magnetic Observatory (HMO) especially to Dr. Lee-Anne McKinnell financial support and hospitality, Prof Peter Kotze for his contagious work ethic and availability were an endless source of encouragement and motivation and data for this research.

Many thanks also to the University of Nairobi for granting me a scholarship for this program and I will always be grateful to the institution. Many people have helped in different capacities to make this research a reality. I cannot mention all of them, but wish to appreciate Dr. Awuor, Mr. Achola, Mr. Odumo, Mr. Obure, Ms. Akinyi Eve for their support and Geoffrey Okeng'o for his special advise and availing programmes that highly supported this dissertation.

I am grateful to all my friends, who are too numerous to mention, for their encouragement during the course of this program. Many thanks to my brother, Mr Antony Orege, my father, Mr. Ochieng Jossy and mother, Aoko Nyogaye, for their understanding and moral support. I appreciate the supports of my in-laws, brothers and sisters. But first, last and always, I would like to thank my darling and sisters, Ms. Jacinter Akoth (Dani) and Hellen Akinyi (Nyoduwa) for thier understanding and encouragement. And finally, Glory to God Almighty Father for seeing me through this program.

Contents

1 Introduction **1**

1.1 The ionosphere 1

1.2 Conductivity and current systems. 3

1.3 Main Objective 9

1.4 Specific Objectives 9

1.5 Justification of the study 9

2 Theoretical Background **11**

2.1 Ionospheric conductivity 11

2.2 Ionospheric current drivers 14

3 Literature Review **16**

4 Methodology **19**

4.1 Data selection and processing. 19

5 Results and Discussion **22**

5.1 January plots 22

5.2 February plots 23

5.3 March plots 25

5.4 April plots 26

5.5 May plots 28

5.6 July plots 29

5.7 August plots 31
5.8 September plots 33
5.9 October plots 34
5.10 November plots 36
5.11 December plots 37
5.12 Interpretation in terms of F-region currents. 40

6 Conclusion and call for further work **46**

DEDICATION

This work is dedicated to my beloved mother, Rosemary Aoko Ogutu (Nyogaye).

List of Figures

1.1.1 Various layers of the ionosphere and their predominant ion populations are listed at their respective heights above ground.The density in the ionosphere varies considerably as shown.Figure from Space Environment Center (SEC) and National Oceanic and Atmospheric Administration (NOAA) by Anderson and Fuller-Rowell, 1999). 2

1.2.1 Typical conductivities for the midlatitude daytime ionosphere (M. Kelly, 1989) . . 3

1.2.2 Plasma populations and magnetospheric current systems (Hermann Lühr et al, 2009) 4

1.2.3 A Schematic representation of E-region dynamo (Schunk and Nagy 2000). 5

1.2.4 Slab geometry 7

1.2.5 Schematic illustration of the F region dynamo over the dip-equator driven by thermospheric winds. Meridional currents systems with opposite sense are set up in the noon and dusk sector (from Lühr and Maus, 2006). 8

4.1.1 Latitudinal regions (Patricia H. Doherty, Satellite Navigation Science and Technology for Africa Workshop, 2009 ICTP, Trieste, Italy) 20

4.1.2 Current sources contributing to the near-Earth magnetic field. Figure adapted from Sabaka et al, 2002 21

5.1.1 X,Y,Z plots of Residuals(nT) vs Latitude(deg),2001/01/6 22

5.1.2 X,Y,Z plots of Residuals(nT) vs Latitude(deg),2001/01/10 23

5.2.1 X,Y,Z plots of Residuals(nT) vs Latitude(deg),2001/02/6 23

5.2.2 X,Y,Z plots of Residuals(nT) vs Latitude(deg),2001/02/11 24

5.2.3 X,Y,Z plots of Residuals(nT) vs Latitude(deg),2001/02/24 24

5.3.1 X,Y,Z plots of Residuals(nT) vs Latitude(deg),2001/03/7 25

5.3.2 X,Y,Z plots of Residuals(nT) vs Latitude(deg),2001/03/12 25

5.3.3 X,Y,Z plots of Residuals(nT) vs Latitude(deg),2001/03/31 26
5.4.1 X,Y,Z plots of Residuals(nT) vs Latitude(deg),2001/04/21 26
5.4.2 X,Y,Z plots of Residuals(nT) vs Latitude(deg),2001/04/26 27
5.4.3 X,Y,Z plots of Residuals(nT) vs Latitude(deg),2001/04/29 27
5.5.1 X,Y,Z plots of Residuals(nT) vs Latitude(deg),2001/05/16 28
5.5.2 X,Y,Z plots of Residuals(nT) vs Latitude(deg),2001/05/16 28
5.5.3 X,Y,Z plots of Residuals(nT) vs Latitude(deg),2001/05/17 29
5.6.1 X,Y,Z plots of Residuals(nT) vs Latitude(deg),2001/07/8 29
5.6.2 X,Y,Z plots of Residuals(nT) vs Latitude(deg),2001/07/26 30
5.6.3 X,Y,Z plots of Residuals(nT) vs Latitude(deg),2001/07/31 30
5.7.1 X,Y,Z plots of Residuals(nT) vs.Latitude(Deg.),2001/08/5 31
5.7.2 X,Y,Z plots of Residuals(nT) vs.Latitude(Deg.),2001/08/8 31
5.7.3 X,Y,Z plots of Residuals(nT) vs.Latitude(Deg.),2001/08/22 32
5.7.4 X,Y,Z plots of Residuals(nT) vs.Latitude(Deg.),2001/08/27 32
5 7.5 X,Y,Z plots of Residuals(nT) vs.Latitude(Deg.),2001/08/30 33
5.8.1 X,Y,Z plots of Residuals(nT) vs Latitude(deg),2001/09/7 33
5.8.2 X,Y,Z plots of Residuals(nT) vs Latitude(deg),2001/09/22 34
5.9.1 X,Y,Z plots of Residuals(nT) vs Latitude(deg),2001/10/15 34
5.9.2 X,Y,Z plots of Residuals(nT) vs Latitude(deg),2001/10/18 35
5.9.3 X,Y,Z plots of Residuals(nT) vs Latitude(deg),2001/10/18 35
5.10.1X,Y,Z plots of Residuals(nT) vs Latitude(deg),2001/11/13 36
5.10.2X,Y,Z plots of Residuals(nT) vs Latitude(deg),2001/11/14 36
5.10.3X,Y,Z plots of Residuals(nT) vs Latitude(deg),2001/11/14 37
5.11.1X,Y,Z plots of Residuals(nT) vs Latitude(deg),2001/12/24 37
5.11.2X,Y,Z plots of Residuals(nT) vs Latitude(deg),2001/12/27 38
5.11.3X,Y,Z plots of Residuals(nT) vs Latitude(deg),2001/12/03 38
5.11.4X,Y,Z plots of Residuals(nT) vs Latitude(deg),2001/12/27 39
5.11.5X,Y,Z plots of Residuals(nT) vs Latitude(deg),2001/12/11 39

5.12.1 Table showing the monthly averaged current densities 41
5.12.2 Monthly average current densities (mA) for Y-component 41
5.12.3 Table showing monthly average current density (mA) for the Z-component 42
5.12.4 Monthly averaged current density (mA) for Z-component 42
5.12.5 Table showing the Average current density (mA) per month for X-component . . . 43
5.12.6 Monthly average current density (mA) for X-component 43
5.12.7 Equatorial anomaly (Doherty, 2009) 44
5.12.8 x-component magnetic field strengths from 2000hrs-2200hrs 45

6.0.1 Dst for 08/08/2001 47
6.0.2 Magnetic elements 48
6.0.3 the seven magnetic components 49

List of Abbreviations

1. nT ..... nanotesla
2. Deg..... Degrees
3. CHAMP..... Challenging Minisatellite Payload
4. Dst index..... Storm-time Disturbance index
5. SEC..... Space Environment Center
6. NOAA..... National Oceanic and Atmospheric Administration
7. EEJ..... Equatorial Electrojet
8. MAGSAT..... Magnetic field Satellite
9. GPS..... Geographical Positioning System
10. OVM..... Overhauser Magnetometer
11. FGM..... Fluxgate Magnetometer
12. EIA..... Equatorial Ionization Anomaly

Chapter 1

Introduction

In this chapter, we briefly describe the ionosphere, its formation, structure and chemical composition. The emphasis is laid on the region of study, the F-region. Further, the ionospheric conductivity and other current systems that exist in the upper atmosphere are outlined. Subsequently the forces that drive these currents, more so, in the F-region such as the dynamos by wind action, gravity gradient and pressure gradient forces are described. Finally, the objectives of the study are outlined followed by the justification.

1.1 The ionosphere

The ionosphere is the part of the earth's upper atmosphere between 70 and1000km where the ions and electrons are present in quantities sufficient to affect the propagation of radio waves [Okeke, 2000]. It makes up less than one percent of the mass of the atmosphere above 70km, nevertheless, it is very important because of its influence on the propagation of High-Frequency radio communication [Anderson and Rowel, 199; Dabas, 2000]. The ionosphere is mostly electrically neutral, but when the solar radiation strikes the chemical constituents of the atmosphere, electrons are dislodged from the atoms and molecules to produce ionospheric plasma. This happens on the sunlit side of the earth by mostly shorter wavelengths of radiation e.g the extreme ultraviolet and X-ray part of the electromagnetic spectrum. The presence of these charged particles make the upper atmosphere an electrical conductor, and it supports electric currents. The charged particles so produced in this process mix with the gas of neutral atoms, thus creating a plasma. A better knowledge of the upper atmosphere must therefore involve an understanding of the distribution and dynamics of this ionospheric plasma which is dependent on complex interaction between the neutral atmospheric winds, solar heating, photo ionization, electrical conductivity and the earth's magnetic field.

The ionosphere has long been divided into regions (D, E, and F), with the term "layer" referring to the ionization within a region. The lowest is the D-region lying at altitudes of about 50 and 90km. The E-region lies between 90 and 160km. Within this region is the normal E layer, produced by solar radiation, and sporadic layers, designated Es caused by the variation of wind speed with height, a wind shear, which, in the presence of geomagnetic field, acts to compress the ionization. Above the E-region lies the F-region within which we have the F1 and F2 layers. The top of the ionosphere is about 1000km, but there is no real boundary between the plasma in the ionosphere and the outer reaches of the Earth's magnetic field, the plasmasphere and the magnetosphere. Figure 1.1.1 shows the ionospheric layers and the principle ions that compose each region.

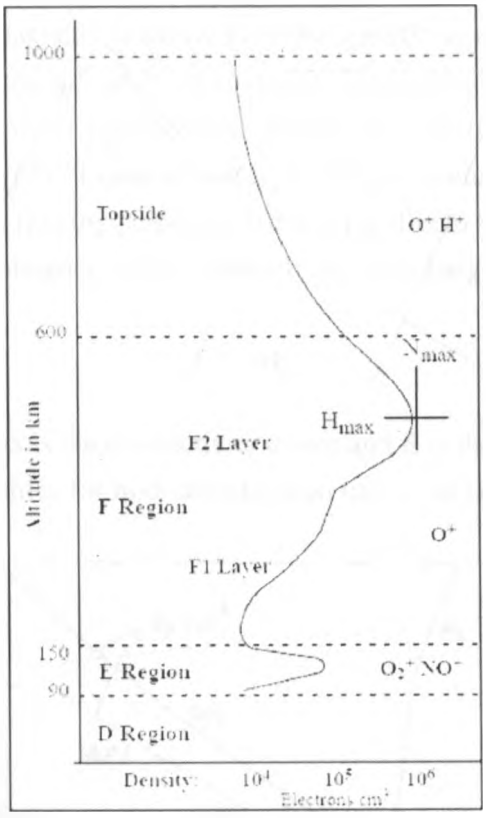

Figure 1.1.1: Various layers of the ionosphere and their predominant ion populations are listed at their respective heights above ground.The density in the ionosphere varies considerably as shown.Figure from Space Environment Center (SEC) and National Oceanic and Atmospheric Administration (NOAA) by Anderson and Fuller-Rowell, 1999).

The F-region does not exhibit the atmospheric mixing processes found in D and E regions and so its composition is determined by ionization production and loss processes, and by diffusive separation of the chemical constituents. In the lower F-region, the main constituents are atomic oxygen and molecular nitrogen. With the increasing altitude, the main constituents change from nitrogen to

atomic oxygen, to helium, and finally to atomic hydrogen. The ionization peaks at the altitude of about 500km to 700km in the F-region where it persists into the night thus supporting the F-region dynamo. Below this peak, the ionization is adversely affected by the rate of plasma production and loss through recombination process.

1.2 Conductivity and current systems.

The ionosphere being an electrical conductor, experiences three types of conductivities depending on the orientation of the electric field to the magnetic field and also varies with the altitude. If the electric field is along the magnetic field, we have the specific or direct conductivity, σ_0, which increases with the increase in altitude and is responsible for the transmission of the electric fields for long distance along the earth's magnetic field. But for the electric fields perpendicular to the magnetic field, we have two types of conductivities; Pedersen conductivity, σ_P, and Hall conductivity, σ_H, to deal with currents flowing perpendicular and parallel to the electric fields respectively. Basically, in the presence of a magnetic field, conductivity of a charged particle is given by Ohm's law,

$$\vec{\mathbf{J}} = \sigma \mathbf{E}$$

where **J** is the current density, σ is the conductivity tensor and **E** is the electric field. A diagram for the calculated conductivity profiles for mid-latitude noon time is as shown below

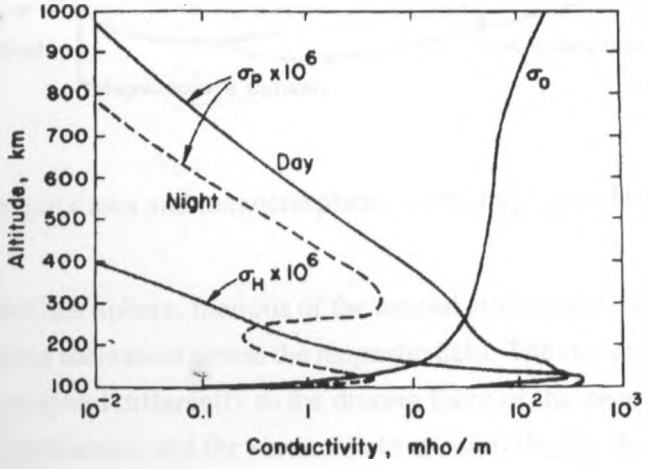

Figure 1.2.1: Typical conductivities for the midlatitude daytime ionosphere (M. Kelly, 1989)

As mentioned before, the upper atmosphere supports electric currents and there are many other current systems, some of which are not in the interest of this study, experienced in the upper atmo-

sphere. A combination of the plasma and electric fields particularly in the magnetosphere allows electric currents to flow. These current systems include:

(i) magnetopause current,

(ii) tail current,

(iii) the ring current (this can be detected by the ground based magnetometers at lower latitudes)

(iv) Birkeland currents (field-aligned currents).

These current systems can best be illustrated using the figure below

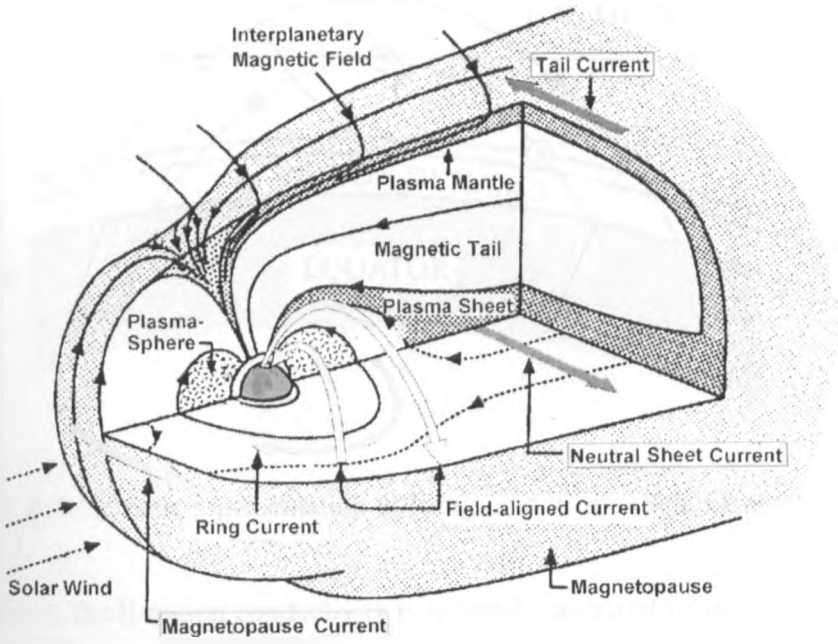

Figure 1.2.2: Plasma populations and magnetospheric current systems (Hermann Lühr et al, 2009)

In E and F regions of the ionosphere, motions of the neutral atmosphere, winds or tides can directly drive currents by dragging ionization across the magnetic field. The current results from the fact that the electrons and ions respond differently to the driving force of the neutral wind. On the dayside, the E-region is highly conductive and the vertical field is controlled by the meridional electric field generated by the global E-region dynamo. This dynamo is driven by the daytime tidal winds. The winds in their motion across the geomagnetic field lines carry along with them the ions while the electrons gyrate more slowly about the magnetic field lines. This relative movement constitutes an electric current and a charge separation produces an electric field, which in turn affects the current. The current system generated in this way is called the S_q, i.e the variation related to the solar day

under quiet geomagnetic conditions [Rabiu, 2001; Rastogi, 2004; Rabiu et al, 2007]. Resulting from this current is an electrostatic field directed east-west (dawn-dusk) in the equatorial dayside of the ionosphere. At the dip equator, where the geomagnetic field is nearly horizontal, this electric field results in an enhanced eastward current flow within $\pm 3^0$of the magnetic equator, known as the equatorial electrojet (EEJ) [Luhr et al, 2004; Rastogi, 2004; Maus et al ,2007; Rabiu et al, 2007; Alken and Maus, 2008]. The equatorial E-region dynamo is illustrated in figure 1.2.3 below.

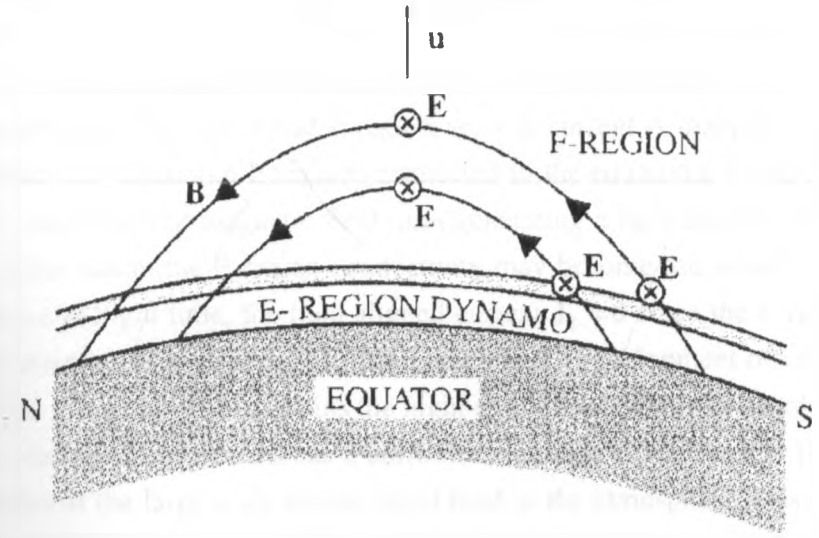

Figure 1.2.3: A Schematic representation of E-region dynamo (Schunk and Nagy 2000).

During the nighttime, the E-region conductivity is reduced considerably and the E-region dynamo loses the control of the ionospheric electrodynamics. The F-region which retains a considerable amount of plasma density exhibit three types of currents namely:

(i) F-region dynamo currents,

(ii) plasma pressure-driven electric currents,

(iii) gravity-driven current system.

In the F-region, κ_j (ratio of gyro frequency to collision frequency) is too large and so the ion and electrons velocities perpendicular to $\mathbf{B}$ are nearly equal. This implies that a plasma flow velocity can be defined uniquely and related to the electric field. The electric fields are majorly generated by the thermospheric winds which also provide the energy that maintains the same at the equatorial region. To give more insight, we redefine our coordinate system to preserve the convectional notation that the $\mathbf{a_z}$ axis is upward. Hence at the equator, we take $\mathbf{B} = \|\mathbf{B}\|\,\mathbf{a_y}$ to be horizontal and northward,

and $\mathbf{a_x}$ towards the east. So the conductivity tensor becomes;

$$\sigma = \begin{pmatrix} \sigma_P & 0 & \sigma_H \\ \sigma_P & \sigma_0 & 0 \\ -\sigma_H & 0 & \sigma_P \end{pmatrix} \tag{1.2.1}$$

The F region dynamo is also driven by the neutral winds which can generate the current while blowing across the magnetic field lines but the mode of operation are different for both of the regions. At the equatorial F region, around the sunrise and sunset, the pressure gradients in the neutral air produce zonal winds which give rise to vertical currents and polarization electric fields on both sides of the terminators. The equatorial F region vertical current is mapped to the magnetically conjugate E region (off equatorial E region) connected to the equatorial F region by the electron flow through the equipotential magnetic field lines generating a field aligned current as shown in Figure 1.2.4a. After sunset the E region conductivity may become too small to support the field aligned currents i.e at night time, the field aligned current $\mathbf{J_y}$ =0 since the E-region ionization is wiped away by recombination processes . This results in the development of vertical polarization electric field at the F region which explains the night time enhancement in zonal plasma drift. The thermospheric wind flowing eastward has a uniform magnitude **U** with height [Kelly, 1989]. The vertical component of the large scale neutral wind field in the atmosphere is usually so small that the wind driven current is vertically upward with magnitude given by $\mathbf{J}_z = \sigma_P \mathbf{UB}$.

As σ_P depends on the product of ionization and collision frequency, $n\upsilon_{in}$, it varies considerably with height and so does the zonal wind component **U**. Thus $d(\sigma_P \mathbf{UB})/d_z \neq 0$ and an electric field must build up in the z direction to produce a divergence free current. In the F region $\sigma_P \gg \sigma_H$ and $\sigma_P \ll \sigma_0$ and thus the horizontal magnetic field lines over the equator bend and enter the E region at high latitudes, which has a finite conductivity. This can be symbolized by the assumption of slab geometry and the F region plasma forms a layer with a well defined lower boundary as shown in figure 1.2.4b below

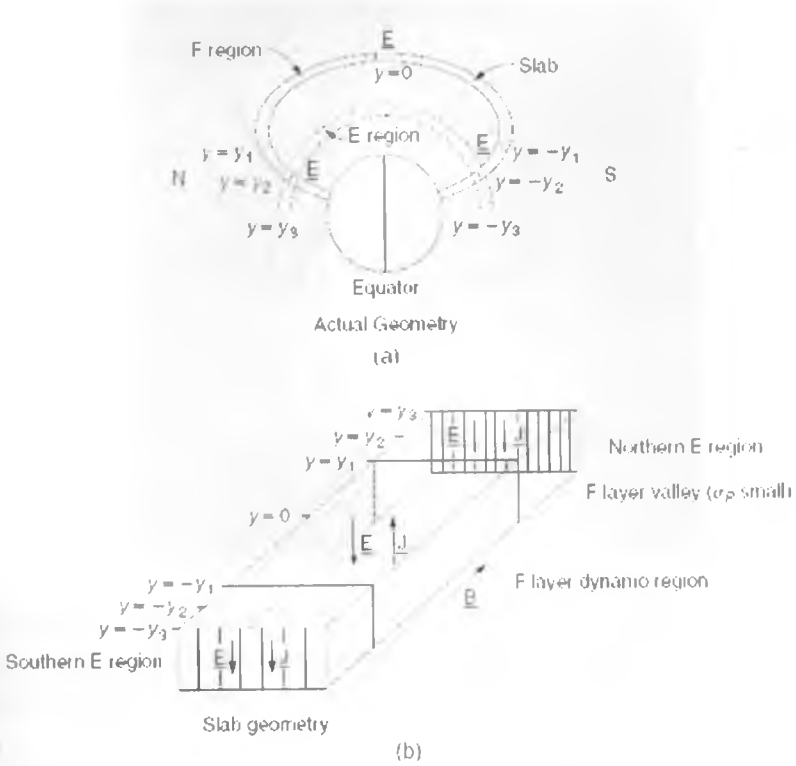

Figure 1.2.4: Slab geometry

The F region plasma has a constant, finite Pedersen conductivity inside the slab and zero elsewhere and zonal wind is constant everywhere. The eastward zonal wind **U** forces the plasma across the magnetic field **B** thus generating a polarization electric field **E**. This gives rise to a zonal drift motion in the F- region plasma. The induced zonal motion in plasma follows the direction as that of the zonal wind i.e. eastward direction in the night. Since the current is upward inside the layer and zero elsewhere, charges pile up at the two boundaries which in turn generates the electric field given by the equation,

$$J_z = \sigma_P E_z + \sigma_P u B = 0$$

which yields

$$E_z = -uB \tag{1.2.2}$$

The mechanism is represented by the pictorial diagram below

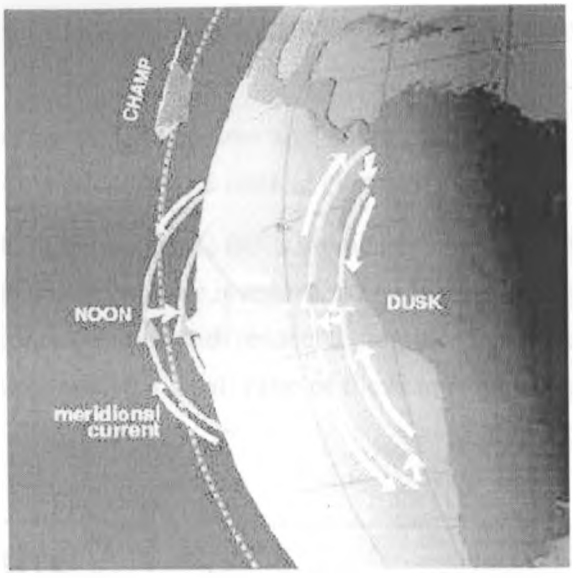

Figure 1.2.5: Schematic illustration of the F region dynamo over the dip-equator driven by thermospheric winds. Meridional currents systems with opposite sense are set up in the noon and dusk sector (from Lühr and Maus, 2006).

Equation (1.2.2) implies that the plasma inside the slab will drift with an $\mathbf{E} \times \mathbf{B}/B^2$ velocity which is equal in magnitude and direction to the zonal wind speed. The insulating end plate assumption is valid mostly in the night time when rapid recombination takes place between molecular ion and electron. The F region dynamo is supported by O^+ ions which are dominant and persist long in the night. However, during the day time, the E region entirely short circuits the magnetic field line integrated F region conductivity and the resulting electric fields are determined by winds in the E region. The E region tidal wind is weak hence the plasma drift is smaller during the day than at night.

Gravity-driven currents systems in the ionospheric F-region create significant magnetic signals that cannot be ignored. Gravitational forces, being omnipresent, produces electric polarization fields in the F-region where Pedersen conductivity is important. It induces an ion motion in the $\mathbf{g} \times \mathbf{B}$ direction hence a charge separation resulting in a current. It is the driving force for the gravitational Rayleigh-Taylor instability which is the basis of the spread F. Plasma pressure-driven electric currents reduce the magnetic field in the equatorial ionospheric anomaly on both sides of the magnetic equator by a few nT. This effect is particularly important for CHAMP, with its orbital altitude close to the peak ionospheric plasma density. These currents are mainly circulating around the regions of enhanced plasma pressure in a away that the magnetic field is reduced in regions of dense plasma i.e in the anomaly regions.

The currents flowing in the ionosphere are affected vastly by a number of factors:

(i) The spatial non-uniformity of the real ionosphere which affect the current through the continuity requirement.

(ii) Time-of-day and latitudinal variations have also some effects while the horizontal layering of the ionosphere has the greatest effect on the vertical currents.

At the magnetic equator where the magnetic fields are nearly horizontal, the ionosphere is bounded in vertical direction. Thus if the ionosphere is regarded as a layer carrying horizontal currents only, it is useful to integrate the conductivities with respect to height. Hence the ability of the ionospheric F region to carry currents depends on a small ratio of the E to F region height-integrated pedersen conductivity.

1.3 Main Objective

To identify the nighttime F-region currents in the equatorial ionosphere over Africa.

1.4 Specific Objectives

- To investigate the F-region currents with respect to pre-midnight and post-midnight sectors.
- To investigate the seasonal variation of the F-region currents.
- To determine the latitudinal variation of the F-region currents.

1.5 Justification of the study

The earth's ionosphere has become the greatest asset for human modern applications ranging from simplest communication to complex space exploration. The earth's ionosphere is very dynamic and most challenging, especially the equatorial region, which is always associated with significant Equatorial Ionization Anomaly structures in the nightside that cannot be the remnants of the same formed during the day. Our study of the ionospheric current systems, which is believed strongly to be associated with this anomaly, equatorial spread F and ionospheric scintillation events, is of much importance as these events are capable of distorting radio communication systems, navigation, space environment monitoring and military defense operations. Our study also reflects the variability of the equatorial ionosphere with distinct distribution of these currents in latitudes longitude (time) which causes adverse effects in high resolution magnetic modeling thus is of much

importance for both the ionospheric and geomagnetic field modelers. Thus we chose, in our study, to understand these dynamics by investigating the possible causes of these currents in the night-side equatorial F-region of the ionosphere 30 degrees north and south of the equator under quiet conditions. This is the first time this kind of study is being carried out over equatorial Africa.

Chapter 2

Theoretical Background

In this chapter, we give, in details, the derivation of the ionospheric conductivity, the possible forces that drive the current in the low-latitude equatorial F-region yielding an equation of the resultant current density in the ionosphere. This equation will come handy in discussion of our results.

2.1 Ionospheric conductivity

The property of a substance to allow the flow of current is called its conductivity. Current results from the motion of the electric charges and the ease with which these charges move is a measure of the conductivity, σ, of the medium carrying the current density, $\mathbf{J}$.

The F-region constitute a partially ionized plasma (neutral and the charges particles) and its plasma constituents respond to the applied forces in such away that there is relative motion between the ions and the electrons resulting in a current whose density is given by:

$$\mathbf{J} = Ne(\mathbf{V}_i - \mathbf{V}_e) \tag{2.1.1}$$

where N is the electron density, e is the elementary charge and $\mathbf{V}_e$ and $\mathbf{V}_i$ are the electron and ion velocities respectively.

Plasma is constituted with different species having their own momentum equation. Here we consider the important body of forces that act on the ionospheric plasma. These forces include:

Gravitational force: $\rho_j \mathbf{g}$

Electric: $n_j q_j \mathbf{E}$

Magnetic: $n_j q_j (\mathbf{V}_j \times \mathbf{B})$

where $n_i = n_e = n$, the plasma density, m is the electron mass, M is the ion mass, T is the temperature, k is Boltzmann's constant, $\mathbf{U}$ the neutral wind and e is the elementary charge. The electric field in the above equations are measured in an earth fixed coordinate system. Transforming these equations in reference frame moving with the neutral flow velocity and assuming that $\|\mathbf{U}\| \ll c$, we have:

$$\mathbf{E}^{'} = \mathbf{E} + \mathbf{U} \times \mathbf{B} \tag{2.1.6}$$

$$\mathbf{B}^{'} = \mathbf{B} - \frac{\mathbf{U} \times \mathbf{E}}{c^2} \tag{2.1.7}$$

where the primed variables are those measured in the moving frame and the unprimed variables are measured in the earth-fixed frame. Equation (2.1.2) can be transformed to a reference frame moving with the neutral wind and since $\mathbf{V}_j^{'} = \mathbf{V}_j - \mathbf{U}$, we have:

$$0 = -k_B T_j \nabla n + nM_j \mathbf{g} + nq_j \mathbf{E}^{'} + nq_j (\mathbf{V}_j^{'} \times \mathbf{B}) - nM_j \upsilon_{jn} \mathbf{V}_j^{'} \tag{2.1.8}$$

Even though the F-region exhibit a collisionless plasma with the plasma velocity perpendicular to $\mathbf{B}$ dominating, the plasma velocity parallel to the same can not be neglected, thus:

$$(\mathbf{V}_\mathbf{j}^{'})_{\shortparallel} = \frac{1}{m_i \upsilon_{jn}} \mathbf{F}_{\shortparallel} + \mathbf{U}_{\shortparallel} \tag{2.1.9}$$

and

$$(\mathbf{V}_\mathbf{j}^{'})_{\perp} = \frac{1}{m_i \upsilon_{jn}} \frac{1}{1 + (\frac{\Omega_j}{\upsilon_{jn}})} \left[\mathbf{F}_\mathbf{j}^{\perp} + \frac{\Omega_j}{\upsilon_{jn}} \mathbf{F}_\mathbf{j}^{\perp} \times \mathbf{b} \right] + \mathbf{U}^{\perp} \tag{2.1.10}$$

where the force $\mathbf{F_j}$ in both equations represents all the force terms independent of the charged particle velocity and $\mathbf{b}$ is the unit vector in the direction of the magnetic field.

By ignoring the pressure and gravitational force terms in the equation (2.1.10) above and evaluating the resultant triple cross-product, we obtain a very important equation showing the drift velocity of collisionless plasma:

$$(\mathbf{V_j})_{\perp} = \mathbf{E} \times \mathbf{B} / B^2 \tag{2.1.11}$$

Now as noted earlier, the ionospheric electrical conductivity depends on the orientation of the electric field to the magnetic field. Thus the ionospheric dynamics is understood by the knowledge of

the altitude variation of the electrical conductivities of the different species. The electrical conductivity is the ratio between current density $\mathbf{J}(A/m)$ and electric field $\mathbf{E}(V/m)$ i.e $\sigma = J/E = Nev/E$, where v is the velocity of the charged particles and N is the particle concentration.

In the absence of a magnetic field or for the electric field along the magnetic field, $\mathbf{B}$, $v = \mathbf{F}/m\upsilon = Ee/m\upsilon$. This implies that $\sigma = Ne^2/m\upsilon$ and in general for both ions and electrons, we have:

$$\sigma_0 = \frac{Ne^2}{m_e \upsilon_e} + \frac{Ne^2}{m_i \upsilon_i} \tag{2.1.12}$$

And for the electric field perpendicular to the magnetic field, we have the Pedersen and Hall conductivity tensors given respectively given by:

$$\sigma_P = Ne^2 \left[\frac{\upsilon_e}{m_e(\upsilon_e^2 + \Omega_e^2)} + \frac{\upsilon_i}{m_i(\upsilon_i^2 + \Omega_i^2)} \right],$$

$$\sigma_H = Ne^2 \left[\frac{\Omega_e}{m_e(\upsilon_e^2 + \Omega_e^2)} - \frac{\Omega_i}{m_i(\upsilon_i^2 + \Omega_i^2)} \right] \tag{2.1.13}$$

2.2 Ionospheric current drivers

The ionospheric current driving forces, gravity-driven currents, pressure gradient currents and F-region dynamo currents, can thus be evaluated from equation (2.1.11) using the fact that $\mathbf{F} = q\mathbf{E}$ as follows:

$$v_j = \sum_j \frac{\mathbf{F_i} \times \mathbf{B}}{q_j B^2} \tag{2.2.1}$$

The gravitational forces exerted on the ions and electrons are $m_i\mathbf{g}$ and $m_e\mathbf{g}$ respectively.From which we have the ion velocity as

$$\mathbf{v_i} = \frac{m_i \mathbf{g} \times \mathbf{B}}{qB^2} \tag{2.2.2}$$

and the electron velocity is ignored due its small mass.

For the pressure gradient force, $\mathbf{F} = \nabla(nkT)$ and this yields the ion and electrons velocities independent of mass as;

$$\mathbf{v_i} = -\frac{\nabla(N_e kT) \times \mathbf{B}}{qB^2}, \mathbf{v_e} = \frac{\nabla(N_e kT) \times \mathbf{B}}{qB^2} \tag{2.2.3}$$

And finally, the drag force between plasma and neutral air is considered where the frictional force term is $m_i \upsilon_{in}(\mathbf{u} - \mathbf{v_i})$, where υ_{ni} is the collision frequency and $\mathbf{u}$ the neutral wind. From the relation, $\mathbf{E} = -\mathbf{v} \times \mathbf{B}$, we get the ion velocity as

$$\mathbf{v_i} = m_i \upsilon_{ni} \frac{\mathbf{E} + \mathbf{u} \times \mathbf{B}}{qB^2} \tag{2.2.4}$$

Thus the resulting current density is:

$$\mathbf{j} = \sigma(\mathbf{E} + \mathbf{u} \times \mathbf{B}) + \{N_e m_i \mathbf{g} \times \mathbf{B} - k\nabla[(T_i + T_e)N_e] \times \mathbf{B}\} \frac{1}{B^2} \tag{2.2.5}$$

where σ is the conductivity tensor, $\mathbf{E}$ is the electric field, $\mathbf{g}$ is the gravitational acceleration, $\mathbf{u}$ is the thermopheric velocity, N_e is the electron density, m_i is the ion mass, k is the Boltzmann constant, $\mathbf{B}$ is the ambient magnetic field and T_e and T_i are the electron and ion temperatures.

Chapter 3

Literature Review

The history of the ionospheric research dates back to 1882 when Balfour Stewart suggested the existence of the ionosphere and since then the Earth's ionosphere has been extensively studied in many aspects over the years using variety of remote and in situ measurements from both ground-based and orbiting platforms, probably because of its role in long-distance communications and broadcasting [Dabas, 2000]

One aspect is the seasonal and magnetic activity variations of nighttime ionospheric F-region vertical plasma drifts. Using the ground-based ionosonde data at Ibadan (an equatorial station in the African zone), this phenomenon has been investigated and the results showed a weak downward F-region motion between ~2100 and ~0500hrs and that the early evening drifts were greater than the post-midnight drift velocities [Oyedemi, 2007]. At the same station, the morphology of the F-region vertical $\mathbf{E} \times \mathbf{B}$ drifts, was investigated in relation to the general characteristics of electrodynamics of the equatorial ionosphere where a profound seasonal and geomagnetic effects were noticed. The F-region drifts show the largest variations in the evening and nighttime periods [Oyedemi and Oluwafemi, 2007]. Surprising new results of F-region irregularities have been observed during the equinox and summer of 2008 that corresponds to low solar activity in which the results revealed remarkably different morphology of the F-region irregularities in summer when compared to that in equinox where in summer, the F-region irregularities were observed as horizontally stratified structures, while in equinox they were observed as plume structures. Further, the irregularities in summer commenced during the post-midnight hours in contrast to their commencement in the post-sunset hours and occurrence extending to post-midnight hours in equinox [Patra and Phanikumar, 2009; Paula et al, 2007].

The low latitude ionosphere has also been studied and modeled. In this respect, the dynamic behavior of the low-latitude ionosphere was presented, the time evolution and spatial distribution of the ionospheric particle densities and velocities were computed by numerically solving the time-

dependent, coupled, nonlinear system of continuity and momentum equations for the various ions taking into account various ionospheric parameters [Bittencourt, 2007].

As one of the most important features of the equatorial ionosphere, the pre-reversal enhancement of the zonal equatorial ionosphere has been investigated and the theories explaining its effects on the equatorial ionosphere are plentiful. From magnetic field observations by CHAMP the estimated pre-sunset F-region dynamo current densities and comparison with PRE velocities given in Fejer et al. (2008) have revealed that the seasonal variation of PRE is consistent with that of the pre-sunset F-region dynamo current strength. Both are largest during equinoxes and smallest during June solstice. The seasonal/longitudinal variations of PRE can also be largely explained by the pre-sunset F-region dynamo currents (R = 0.74). Thus the acceptance that the F-region dynamo drives the pre-reversal enhancement of vertical plasma drift (PRE) near sunset. The observations provided confirmation for the close relationship between the F-region dynamo current density and PRE [Park et al, 2010; Nayar et al, 2009 and Kelly et al, 2009].

The literature on equatorial ionosphere irregularities such as Scintillation, Spread-F and plasma bubbles are also adequate [Subbarao and Murthy, 1993; Sastri, 1999; Sinha and Raizada, 2000; Niranjan et al, 2002; Xiaoqing Pi et al, 2003; Martinis et al, 2005 Chu et al, 2005; Ram et al, 2006;Arruda et al, 2006; Yokoma and Fukao 2006; Yao and Makela, 2007; Oyekola, 2009; Olwendo et al, 2009; Takahashi et al, 2009; Abdu et al, 2009; Yang et al, 2010].

The electric fields in the equatorial ionosphere has also been studied [Shume et al, 2009]. The day time eastward equatorial electric field (EEF) in the E-region plays an important role in equatorial ionospheric dynamics. It is responsible for driving equatorial electrojet (EEJ) current system, equatorial vertical ion drifts, and the equatorial ionization anomaly (EIA) [Maus et al, 2007; Alken and Maus, 2008]. Other than interpreting magnetic signatures from CHAMP satellite to investigate the average features and global characteristics of the EEJ, a horizontal current distribution has been determined by using a very general current model-series of line currents. The results have shown that the electrojet currents peak right at the dip equator and there is no deviation from it either on a seasonal basis or with longitude [Luhr et al, 2004].

Investigations of the day side F-region have revealed the existence of reverse currents at the flanks of the primary eastward current and more importantly the average characteristics of the F-region driven currents were observed for the first time throughout the day. The meridional current system, driven by the westward thermospheric winds, peaks around noon while similar currents but flowing in the opposite direction were observed at the dusk sector [Park et al, 2010; Luhr and Maus,2006; Sager and Huang, 2002].

So far little has been done about the direct current measurement in the F-region, probably because of the weak magnetic effect they cause and thus can be easily masked by other variations.

The CHAMP satellite with its precision high magnetic field measurements have been employed to detect and characterize the tropical F-region ionospheric currents on the earth's nightside for the first time using the scalar data from CHAMP overhauser magnetometer. The results revealed a height-integrated current density estimated to be of the order of 5 mA/m spatially confined to the near-equatorial region bounded by the Appleton anomaly and their appearances in the pre-midnight sector but could not find the relation between the current intensity and magnetic activity within the limited range of (Kp = 0 . . .2). The study also showed that the current signatures are generally accompanied by small- scale (%100 km) intensity fluctuations which could be associate with fluctuations with spread F features. The occurrence distribution of the F region currents with longitude shows a clear peak in the Atlantic sector, a minimum in the Indian sector and intermediate rates over the Pacific. This pattern resembles very closely the distribution of F region instabilities [Luhr et al, 2002].

In this study, an investigation of, in-situ F-region current from the the nightside equatorial zone using the vector data from the CHAMP Fluxgate Magnetometers is presented.

Chapter 4

Methodology

The Challenging Minisatellite Payload (CHAMP) satellite was launch on 15th July, 2000 into an almost circular orbit, near-polar (inclination=87.3^0) orbit with an initial altitude of about 450km. The primary mission objectives are studies related to the gravity fields, magnetic field and the atmosphere. The satellite CHAMP in its low-latitude polar orbit and its high magnetic field measurements provides the best opportunity to study and investigate ionospheric currents in greater details. With its high inclination orbit, CHAMP covers all the local times as opposed to Magnetic Field Satellite, MAGSAT (1979-1980). Flown on the satellite are greatly advanced instruments, such as: Star Accelerometer, GPS Receivers (combined with the STAR accelerometer, serves as the main tool for high-precision orbit determination of the CHAMP satellite), Digital Ion Drift Meter (mainly used to make in-situ measurements of the ion distribution and its moments within the ionosphere), Overhauser Magnetometer (OVM) which serves as the magnetic reference for the CHAMP mission. It samples continuously the ambient field strength at a rate of 1 Hz thus provides an absolute in-flight calibration capability for the Fluxgate Magnetometer vector magnetic field measurements. A dedicated program ensuring the magnetic cleanliness of the spacecraft allows for an absolute accuracy of the readings of < 0.5 nT and Fluxgate Magnetometer (FGM) which probes the vector components of the Earth magnetic field covering full range of the Earth's field, ±65 000 nT, in all three components hence the prime instrument for the magnetic field investigations of the CHAMP mission.

4.1 Data selection and processing.

The CHAMP raw vector data (X, Y, Z), measured by the Fluxgate Magnetometer were selected between 30 deg North and 30 deg South in latitude, and between 35 and 40 deg East. The region is shown in the figure 4.1.1 below

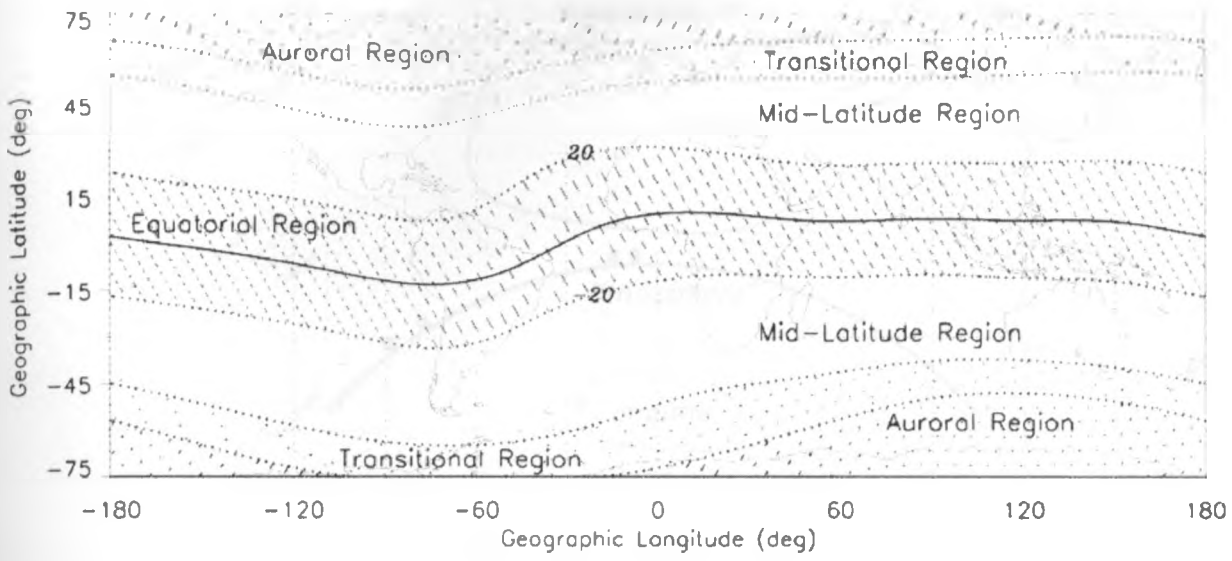

Figure 4.1.1: Latitudinal regions (Patricia H. Doherty, Satellite Navigation Science and Technology for Africa Workshop, 2009 ICTP, Trieste, Italy)

The night time (20h00 – 05h00 LT) data measured during the year 2001 on quiet-time of Storm time Disturbance (Dst), less than 15 were utilized to eliminate the effects of the E-region and storm-time contributions. The Fluxgate Magnetometer, as mentioned before, samples all the three components of the field at 50Hz with a resolution of 0.1nT over a range of $\pm 65,000$ nT. For high accuracy, the Fluxgate data are routinely calibrated against the absolute scalar Overhauser readings.

The satellite makes several passes through the equator in a 24hour period. The data for a total of 306 passes were collected for our study.

The quantity of interest in this study is the night side ionospheric currents as deduced from the magnetic field that they generate at the earth's surface. Before we single out this particular effect, we note that the terrestrial magnetic field is composed of contributions from many sources.

These sources include and are also diagrammatically shown in the figure 4.1.2 below

(i) the earth's core,

(ii) the earth's crust,

(iii) ionosphere,

(iv) the magnetosphere, and

(v) the from coupling currents between the ionosphere and the magnetosphere, and between hemispheres.

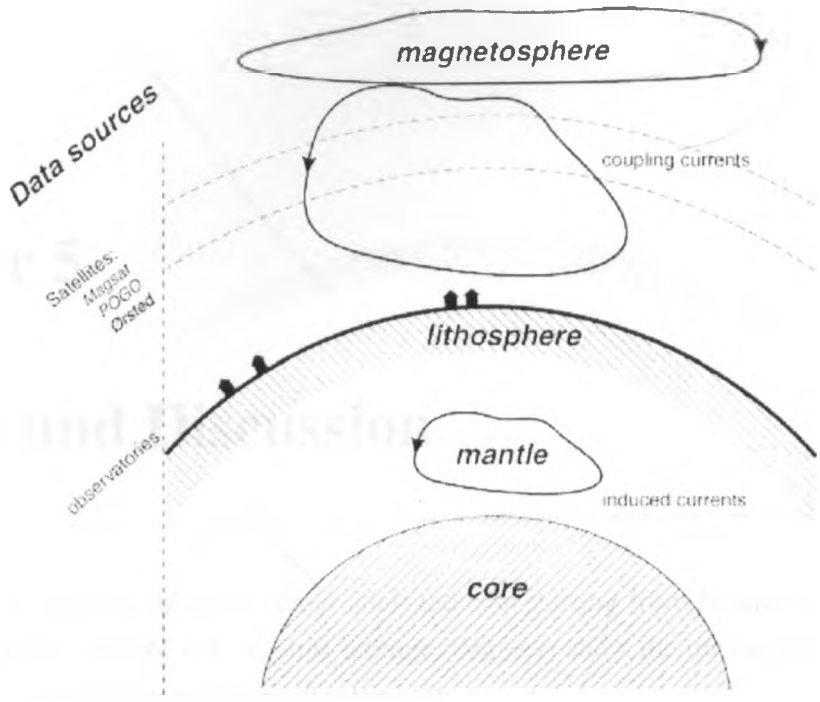

Figure 4.1.2: Current sources contributing to the near-Earth magnetic field. Figure adapted from Sabaka et al, 2002

The processing of the data was done on the fortrun programme upon which all the field models; main field, crustal field, epoch and spline fitting models were embedded.

The raw data was first ran on the epoch programme which rearranged the data in columns beginning from year, month, day, latitude, longitude, altitude, x, y, and z components.

The day time data were discarded leaving us with only the nighttime data with total of 189 passes. Thereafter, the data for the days with the Dst index more than 15 were also eliminated and only data for 89 passes were considered and plotted for this study.

Next, the earth's main field contributions which is the primary source, accounting for over 97 per cent of the field observed at the earth's surface with intensity ranging from about 30 000 nT at the equator to about 50 000 nT at the poles, was eliminated by running the data on the main field model programme, International Geomagnetic Reference Field (IGRF). This earth's main magnetic field can be described using Gauss coefficients derived from a spherical harmonic analysis and for our case, we separate each model main field into a core field (harmonics of degrees 1–13, with its secular variation), and a lithospheric field or crustal field (degrees 14-90).

Finally to remove the ring currents, we did a spline fit to the X, Y and Z residuals, and subtracted to leave us with only external field contributions resulting from F region currents.

Chapter 5

Results and Discussion

In this chapter, we present the plots of our analyzed data starting from January to December. The plots of the magnetic residue (nT) against latitude (degrees) show the magnitude of magnetic signatures that are used in the discussion after the plots.

5.1 January plots

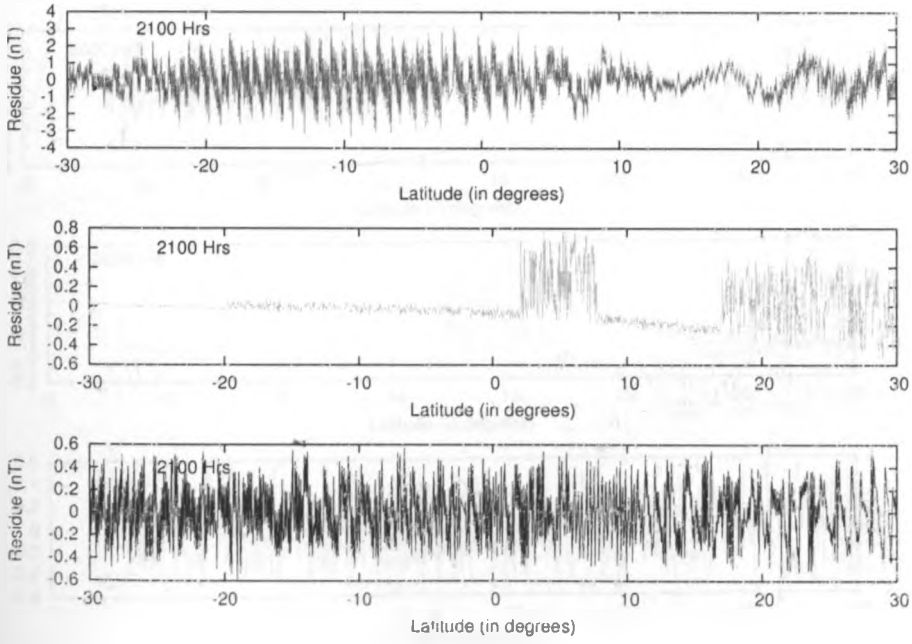

Figure 5.1.1: X,Y,Z plots of Residuals(nT) vs Latitude(deg),2001/01/6

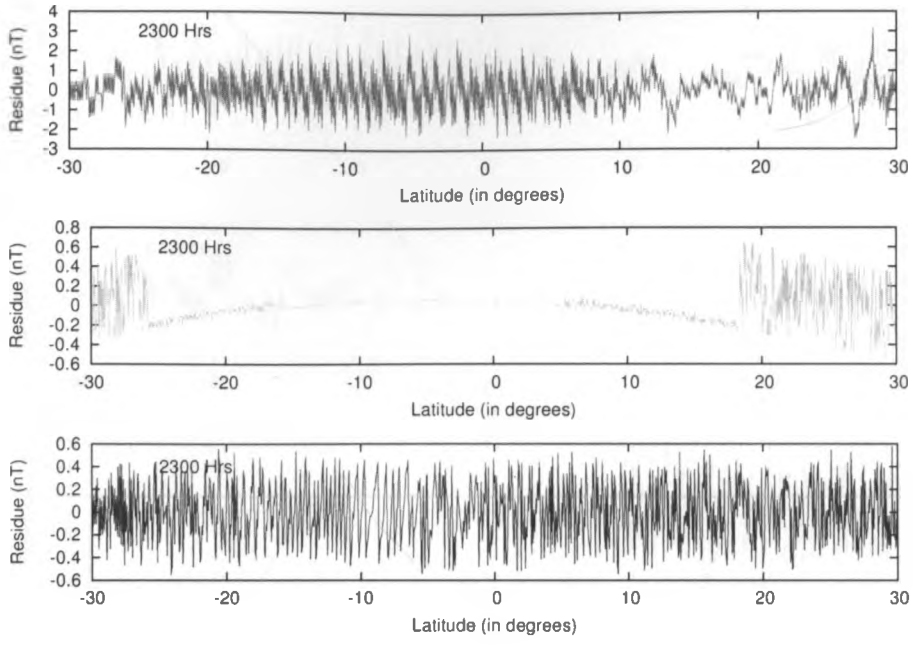

Figure 5.1.2: X,Y,Z plots of Residuals(nT) vs Latitude(deg),2001/01/10

5.2 February plots

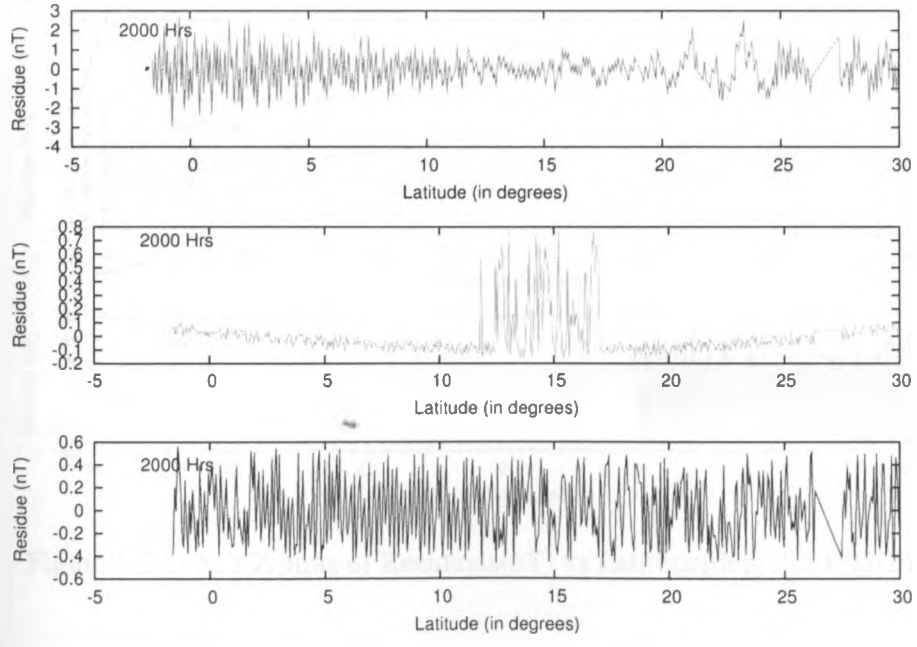

Figure 5.2.1: X,Y,Z plots of Residuals(nT) vs Latitude(deg),2001/02/6

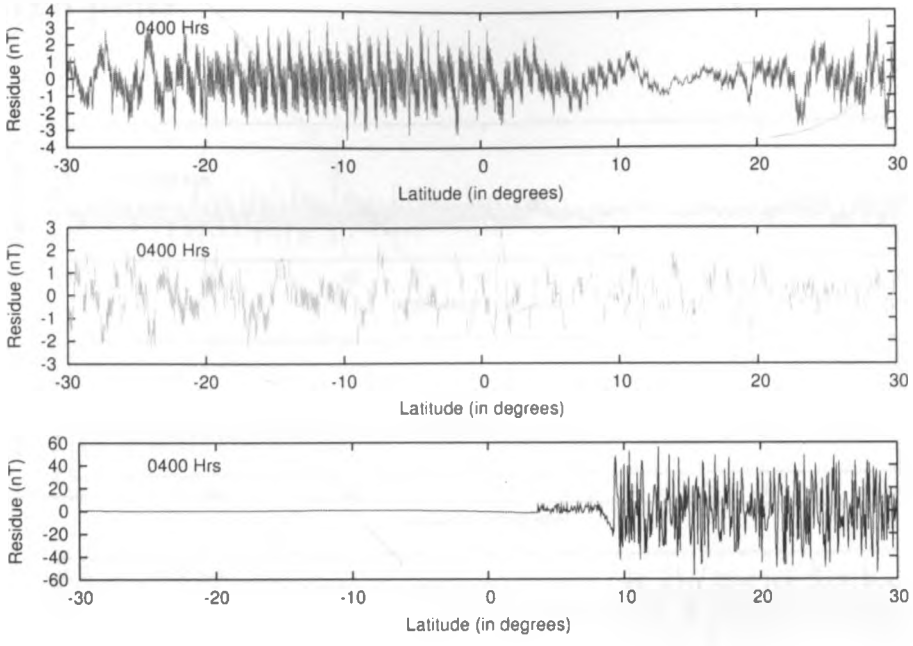

Figure 5.2.2: X,Y,Z plots of Residuals(nT) vs Latitude(deg),2001/02/11

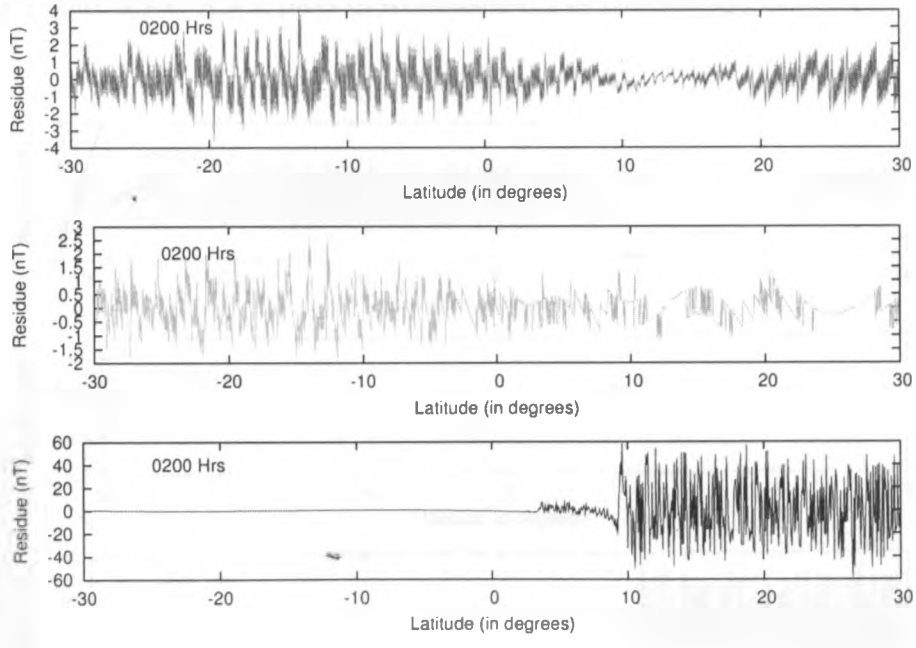

Figure 5.2.3: X,Y,Z plots of Residuals(nT) vs Latitude(deg),2001/02/24

5.3 March plots

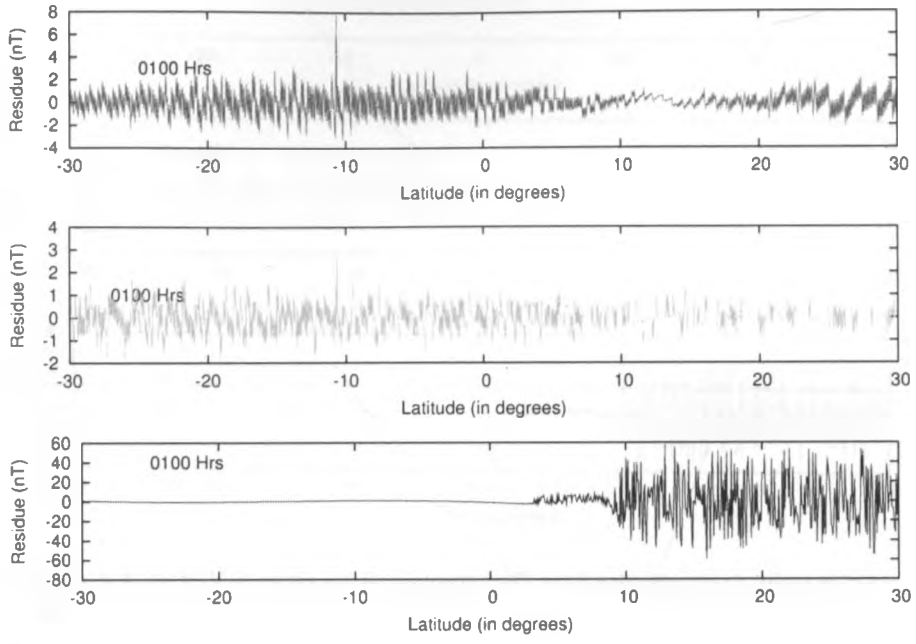

Figure 5.3.1: X,Y,Z plots of Residuals(nT) vs Latitude(deg),2001/03/7

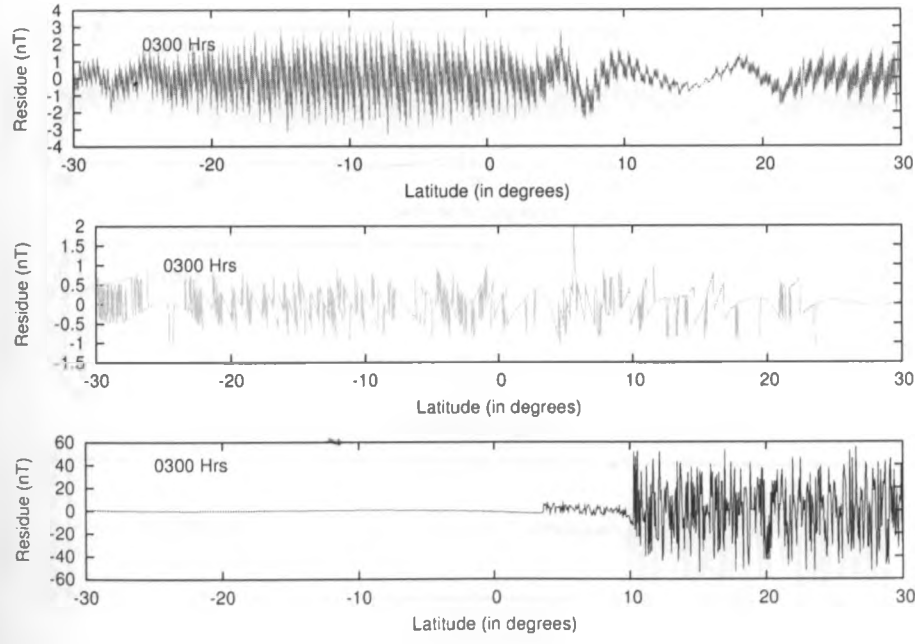

Figure 5.3.2: X,Y,Z plots of Residuals(nT) vs Latitude(deg),2001/03/12

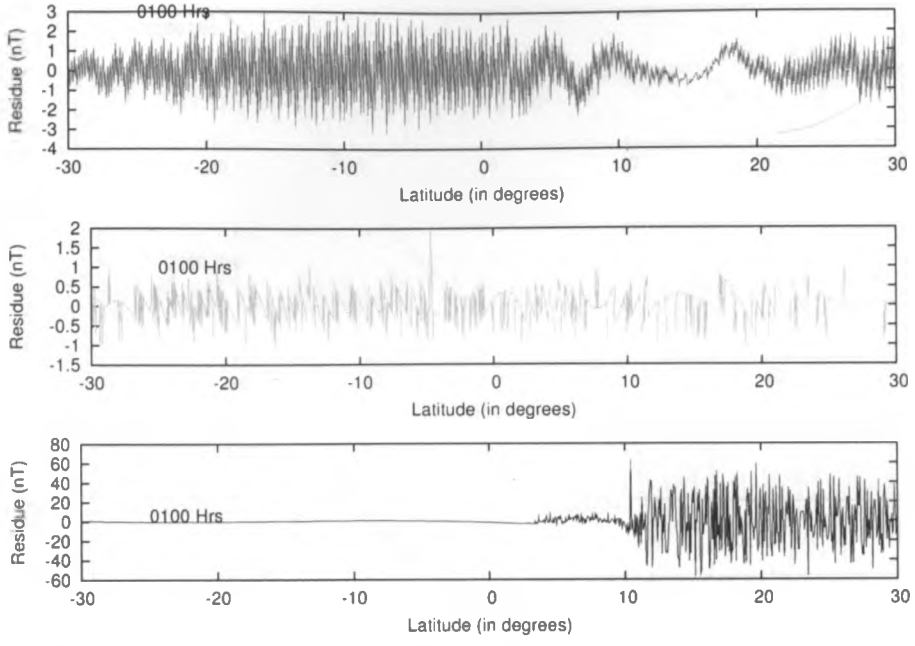

Figure 5.3.3: X,Y,Z plots of Residuals(nT) vs Latitude(deg),2001/03/31

5.4 April plots

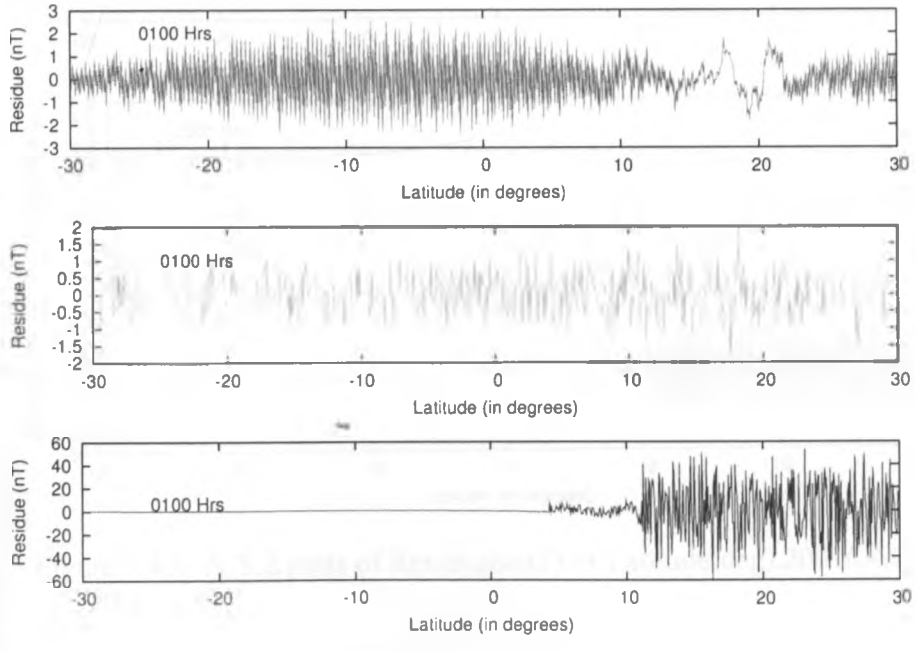

Figure 5.4.1: X,Y,Z plots of Residuals(nT) vs Latitude(deg),2001/04/21

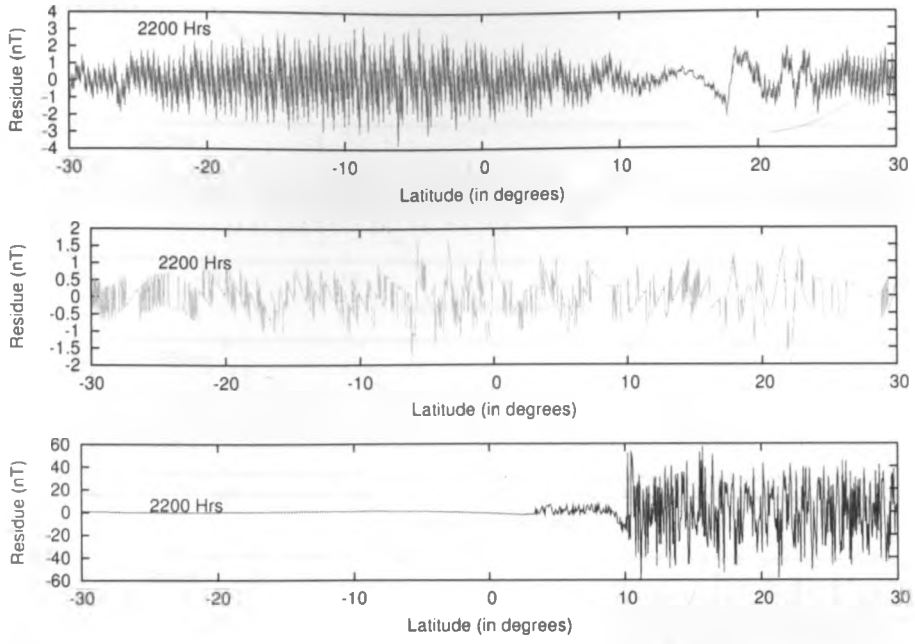

Figure 5.4.2: X,Y,Z plots of Residuals(nT) vs Latitude(deg),2001/04/26

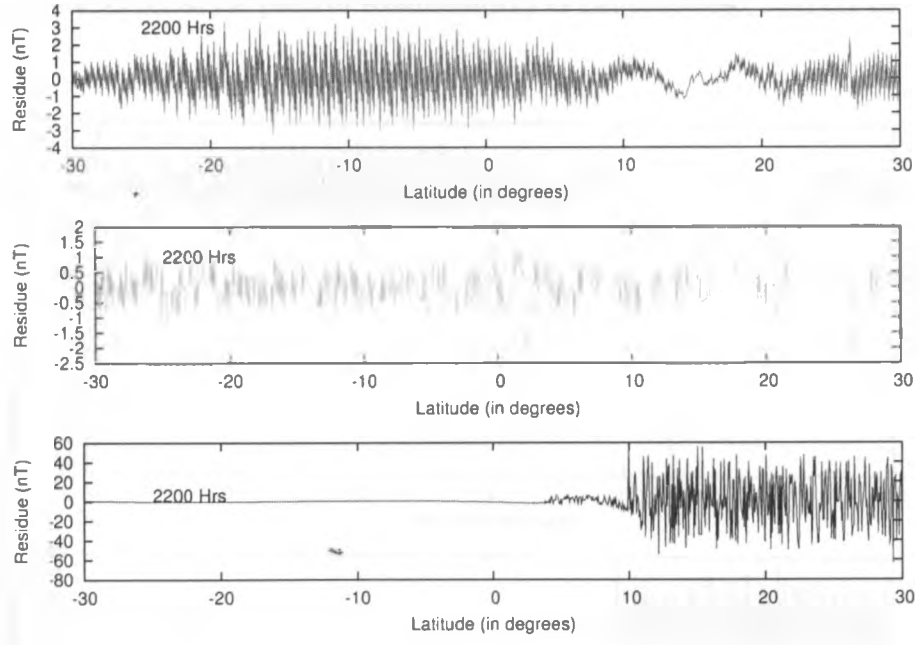

Figure 5.4.3: X,Y,Z plots of Residuals(nT) vs Latitude(deg),2001/04/29

5.5 May plots

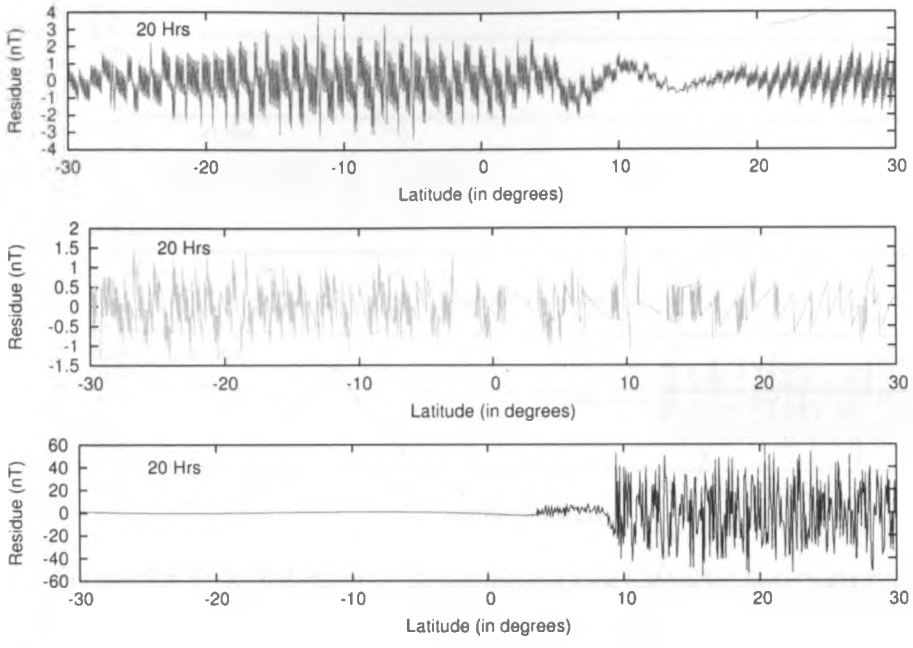

Figure 5.5.1: X,Y,Z plots of Residuals(nT) vs Latitude(deg),2001/05/16

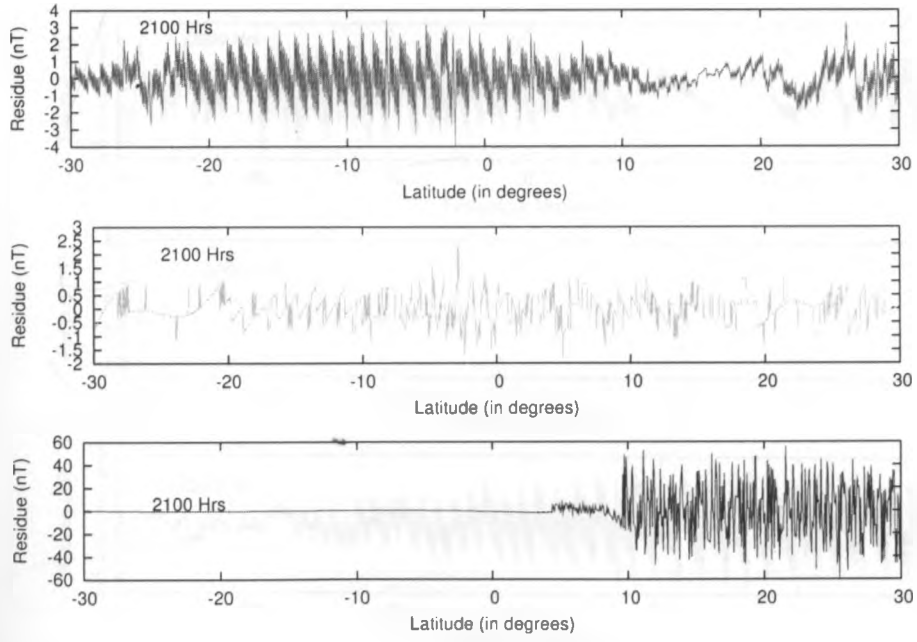

Figure 5.5.2: X,Y,Z plots of Residuals(nT) vs Latitude(deg),2001/05/16

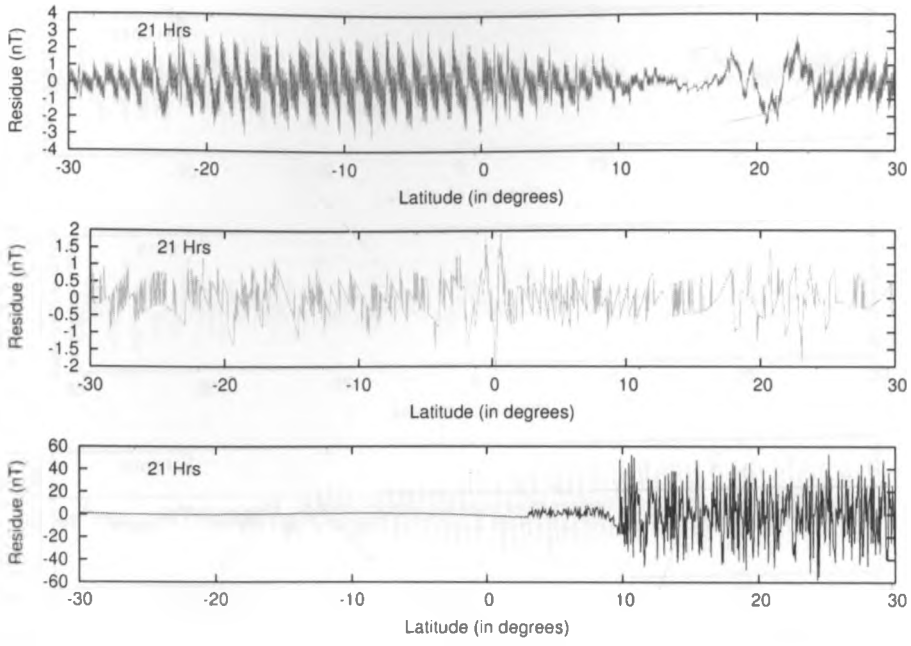

Figure 5.5.3: X,Y,Z plots of Residuals(nT) vs Latitude(deg),2001/05/17

5.6 July plots

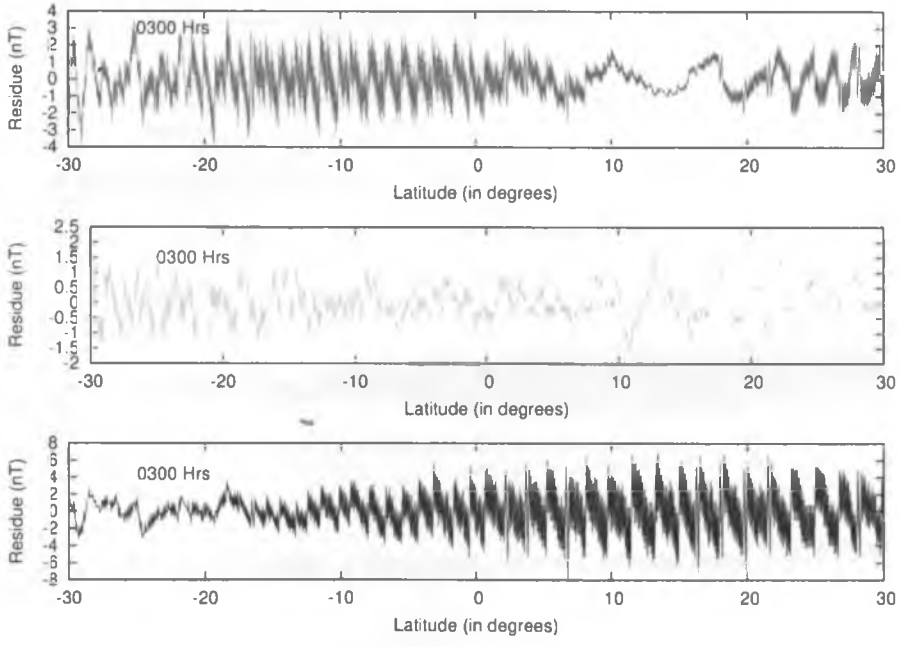

Figure 5.6.1: X,Y,Z plots of Residuals(nT) vs Latitude(deg),2001/07/8

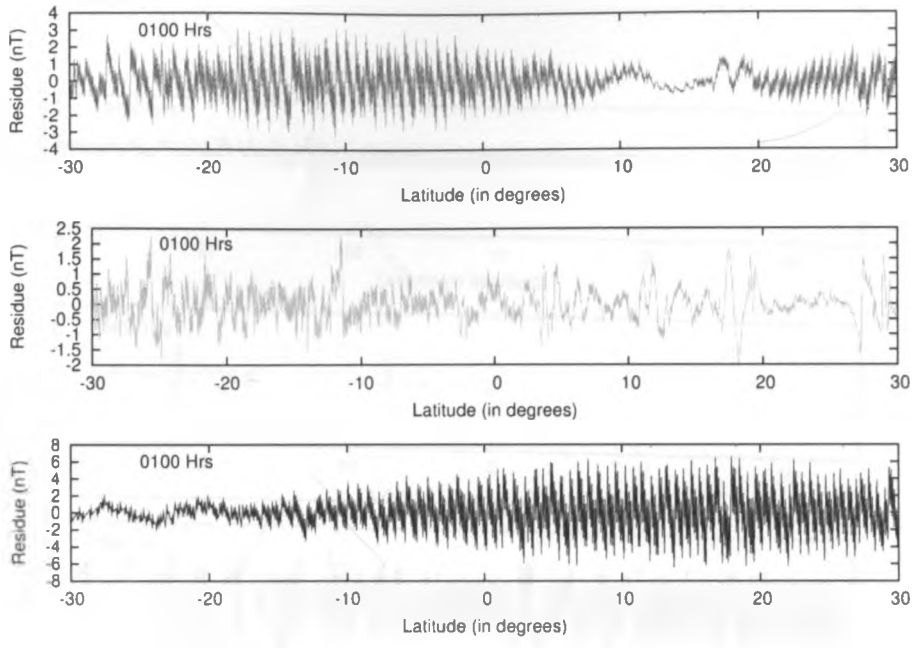

Figure 5.6.2: X,Y,Z plots of Residuals(nT) vs Latitude(deg),2001/07/26

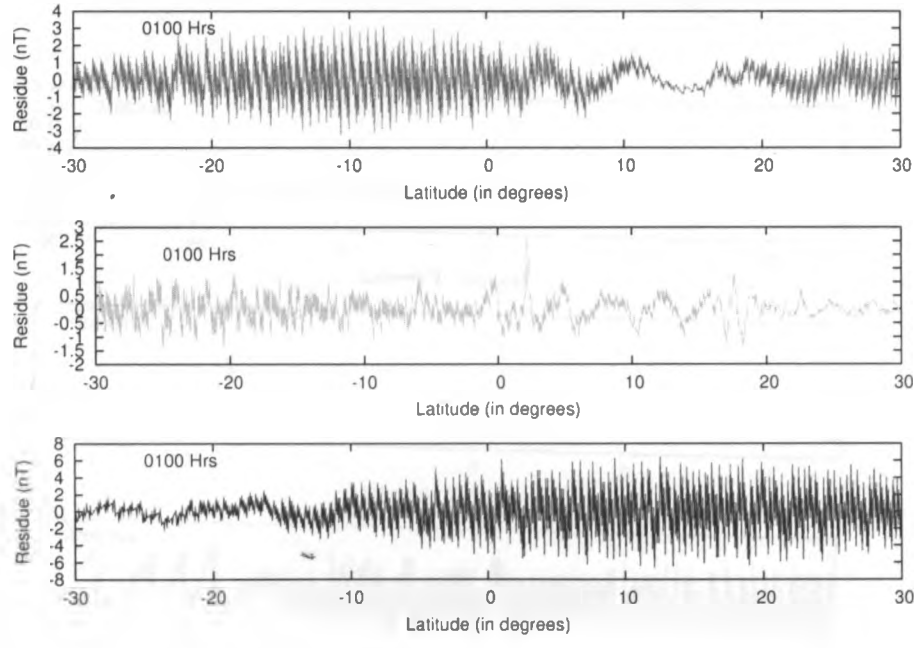

Figure 5.6.3: X,Y,Z plots of Residuals(nT) vs Latitude(deg),2001/07/31

5.7 August plots

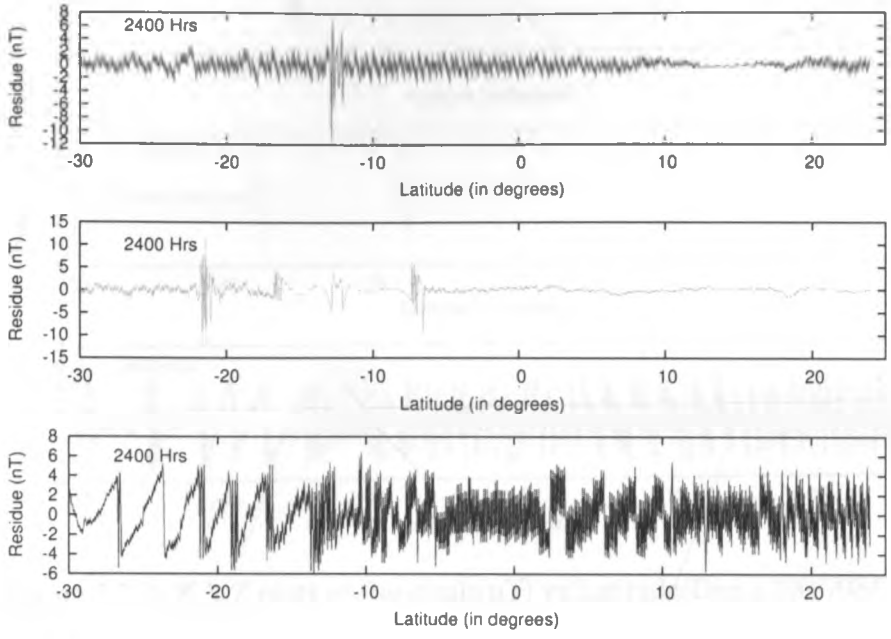

Figure 5.7.1: X,Y,Z plots of Residuals(nT) vs.Latitude(Deg.),2001/08/5

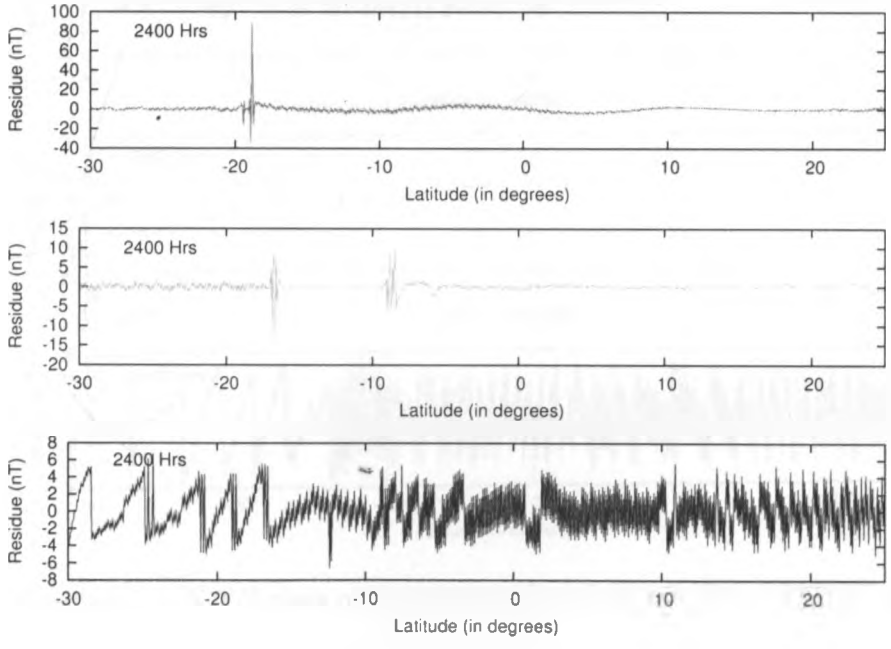

Figure 5.7.2: X,Y,Z plots of Residuals(nT) vs.Latitude(Deg.),2001/08/8

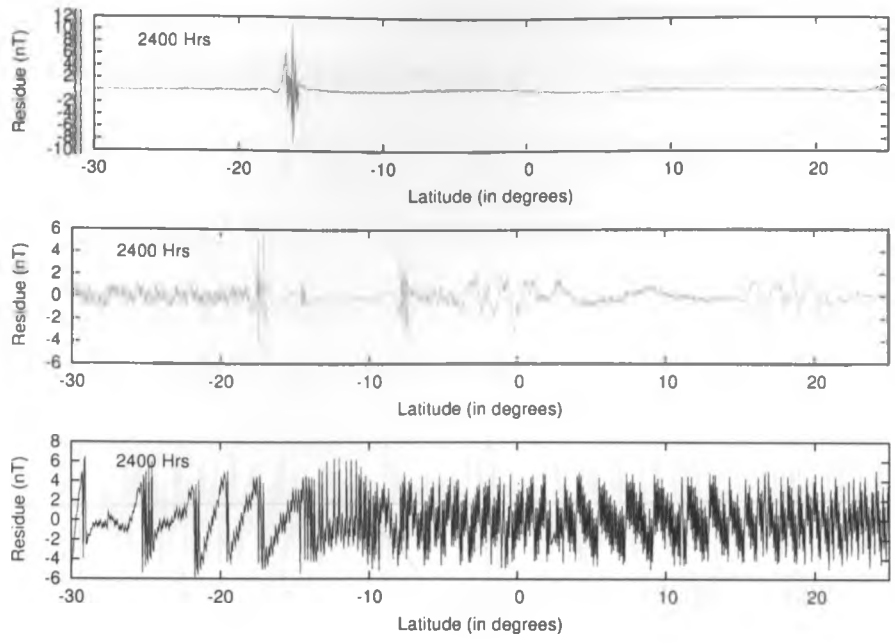

Figure 5.7.3: X,Y,Z plots of Residuals(nT) vs.Latitude(Deg.),2001/08/22

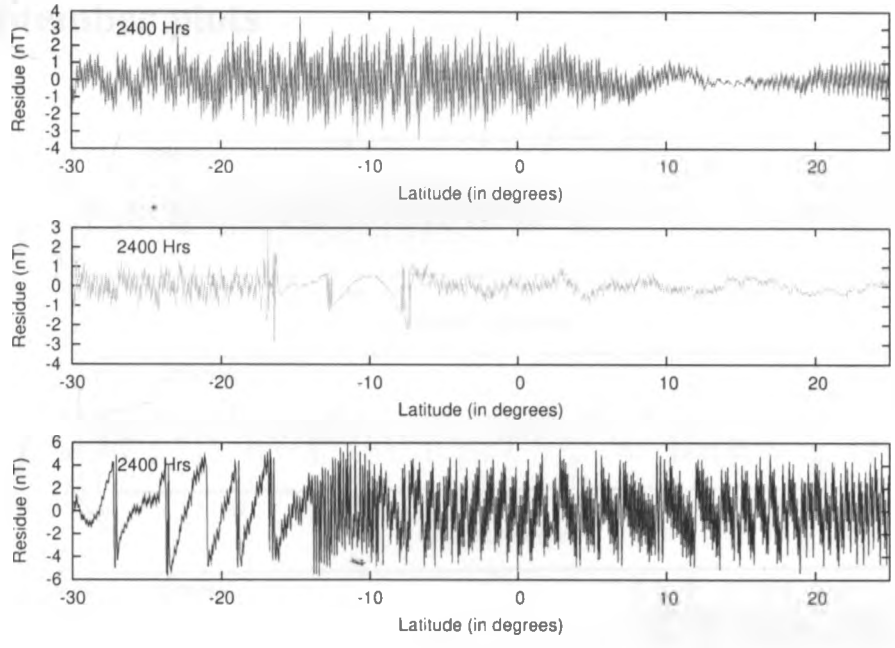

Figure 5.7.4: X,Y,Z plots of Residuals(nT) vs.Latitude(Deg.),2001/08/27

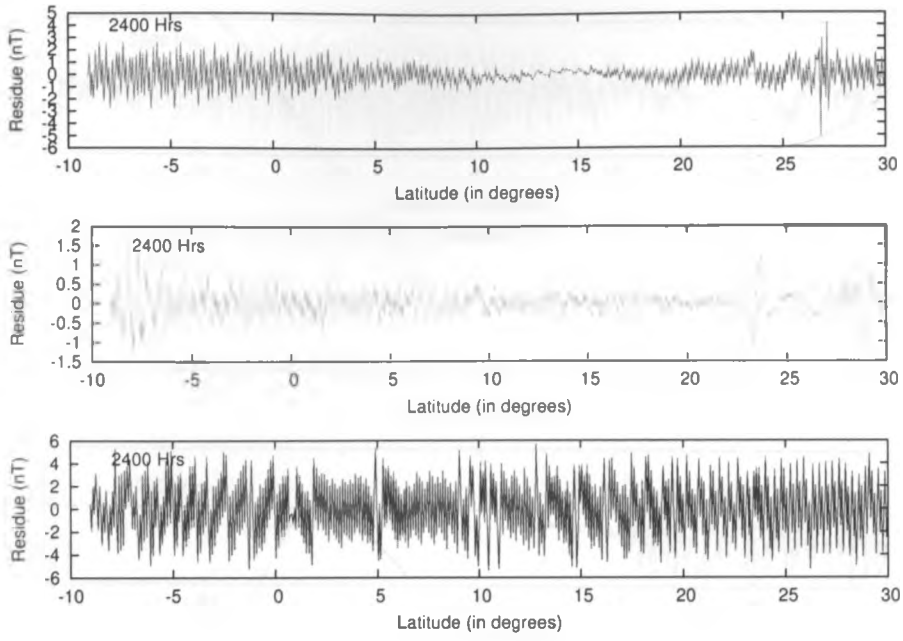

Figure 5.7.5: X,Y,Z plots of Residuals(nT) vs.Latitude(Deg.),2001/08/30

5.8 September plots

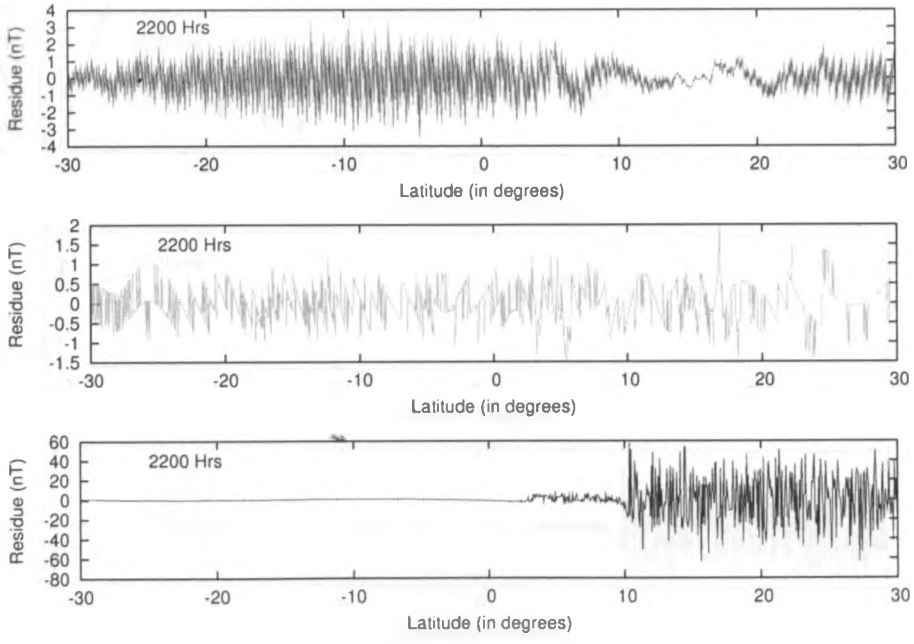

Figure 5.8.1: X,Y,Z plots of Residuals(nT) vs Latitude(deg),2001/09/7

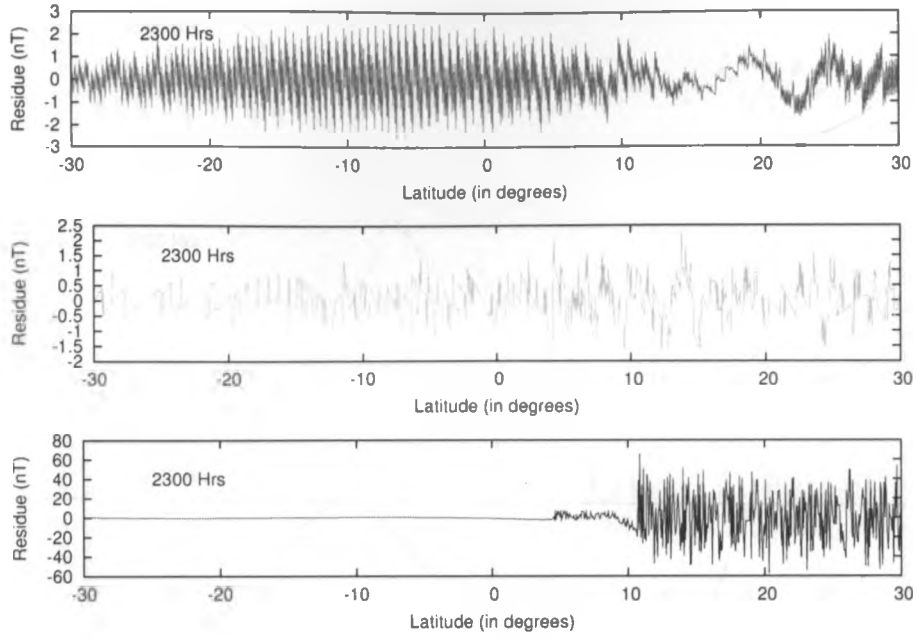

Figure 5.8.2: X,Y,Z plots of Residuals(nT) vs Latitude(deg),2001/09/22

5.9 October plots

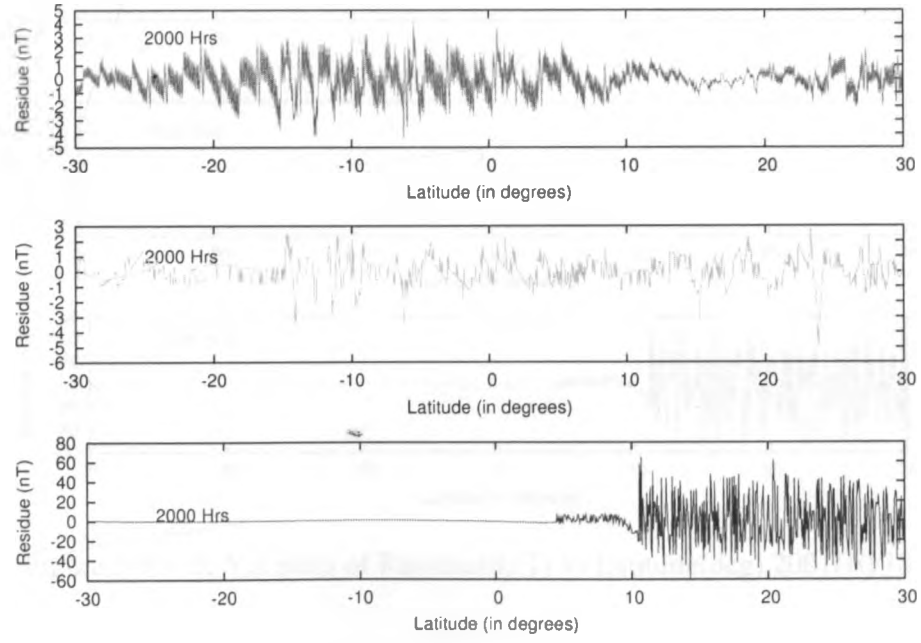

Figure 5.9.1: X,Y,Z plots of Residuals(nT) vs Latitude(deg),2001/10/15

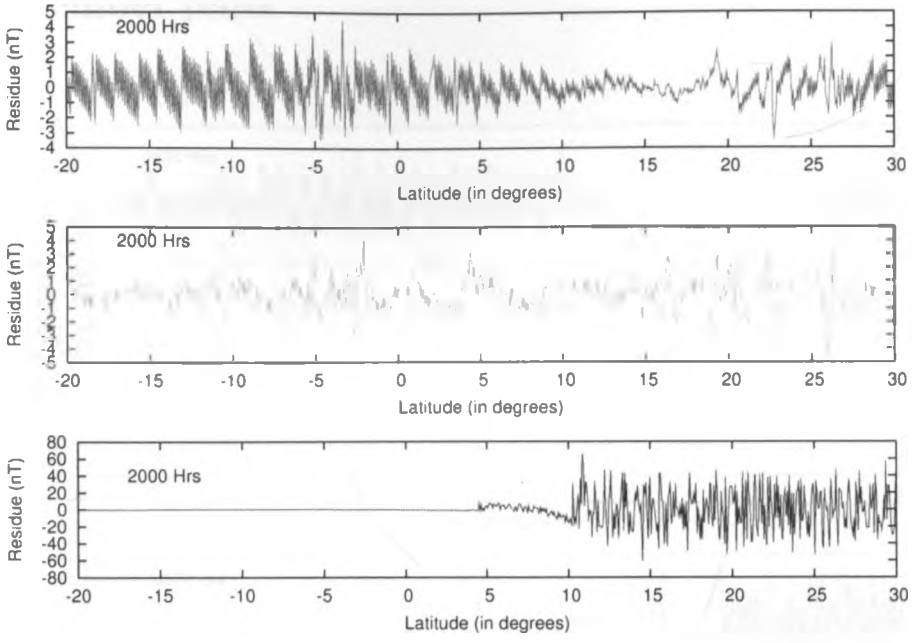

Figure 5.9.2: X,Y,Z plots of Residuals(nT) vs Latitude(deg),2001/10/18

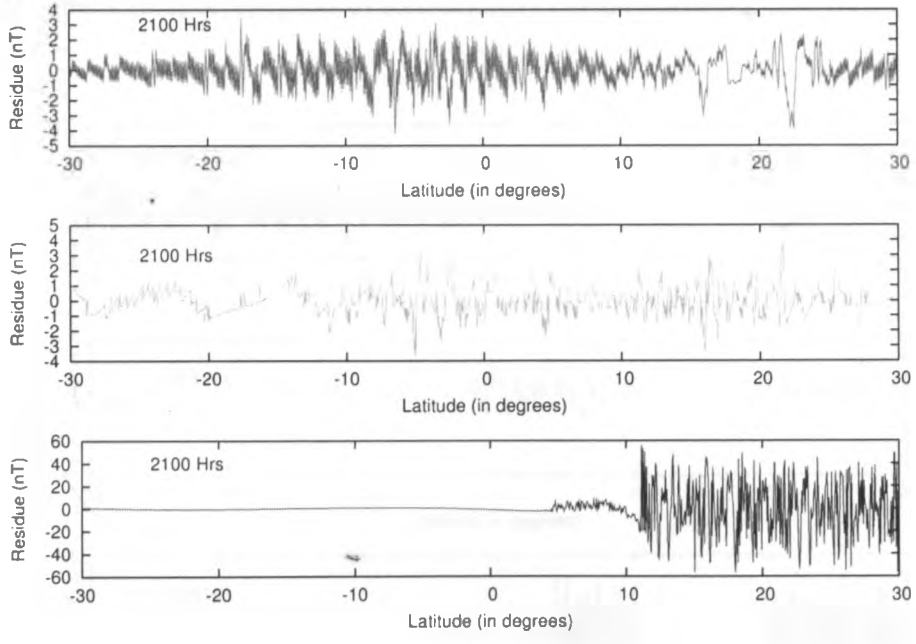

Figure 5.9.3: X,Y,Z plots of Residuals(nT) vs Latitude(deg),2001/10/18

5.10 November plots

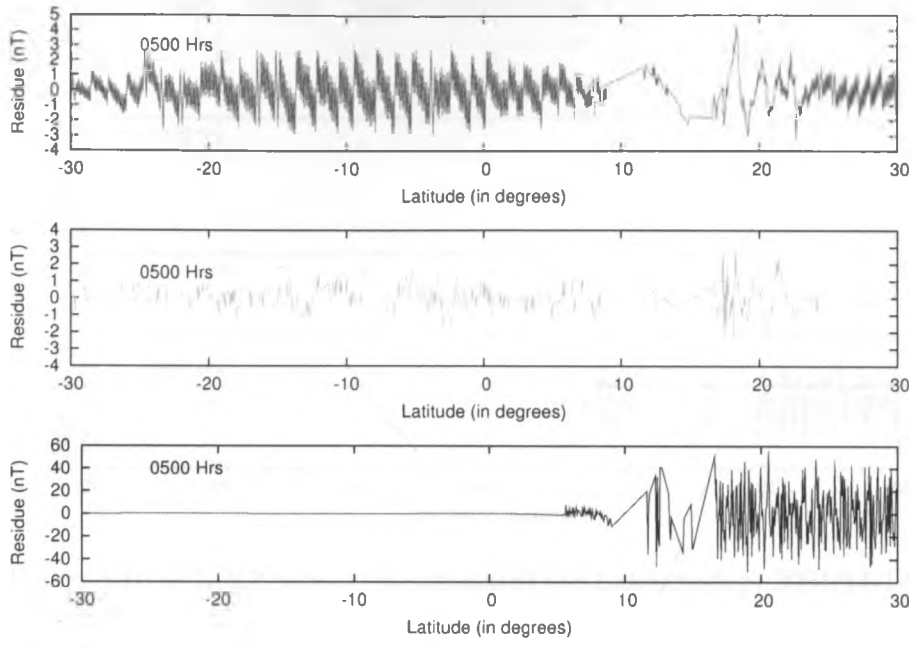

Figure 5.10.1: X,Y,Z plots of Residuals(nT) vs Latitude(deg),2001/11/13

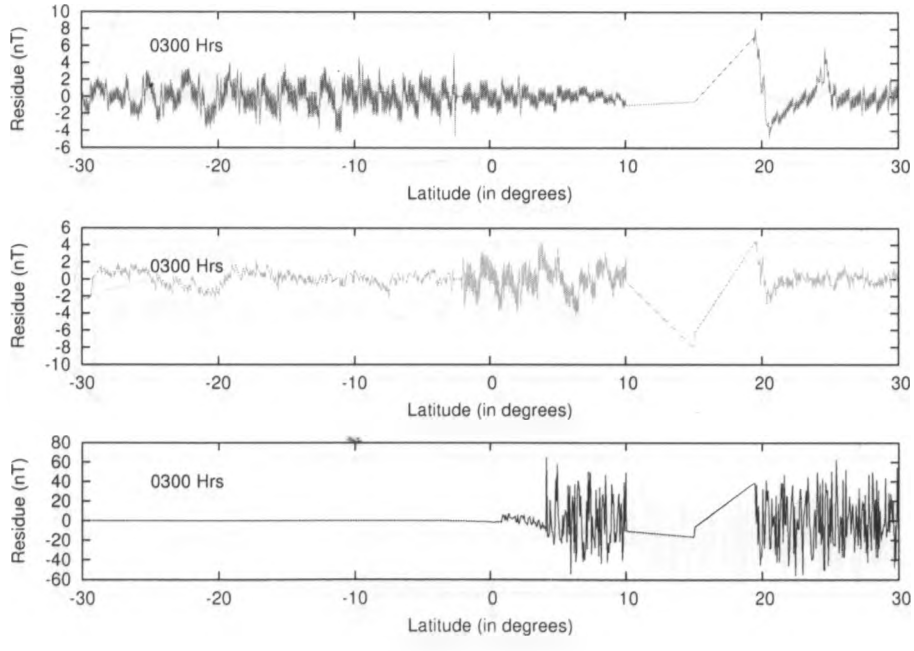

Figure 5.10.2: X,Y,Z plots of Residuals(nT) vs Latitude(deg),2001/11/14

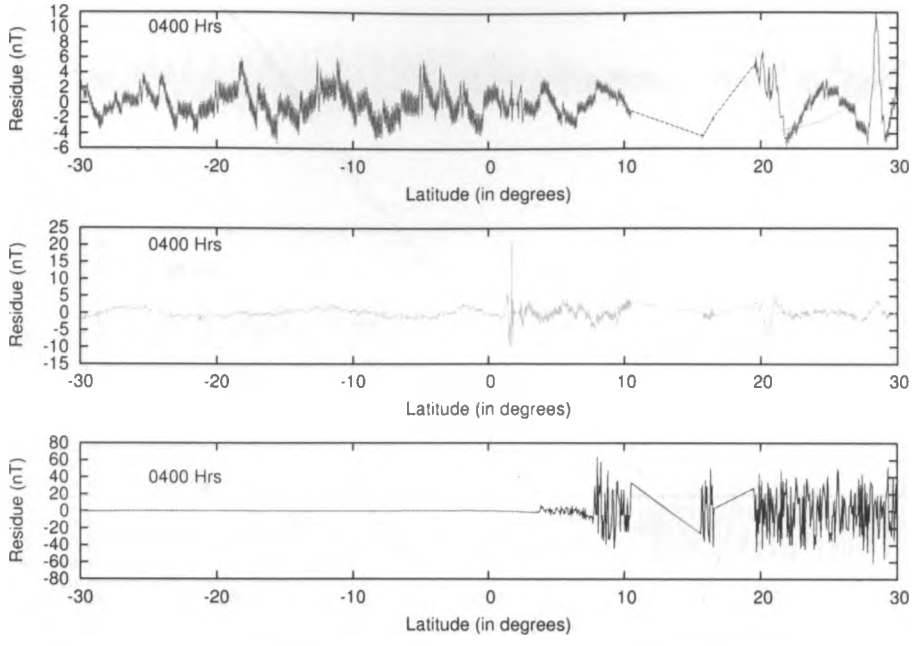

Figure 5.10.3: X,Y,Z plots of Residuals(nT) vs Latitude(deg),2001/11/14

5.11 December plots

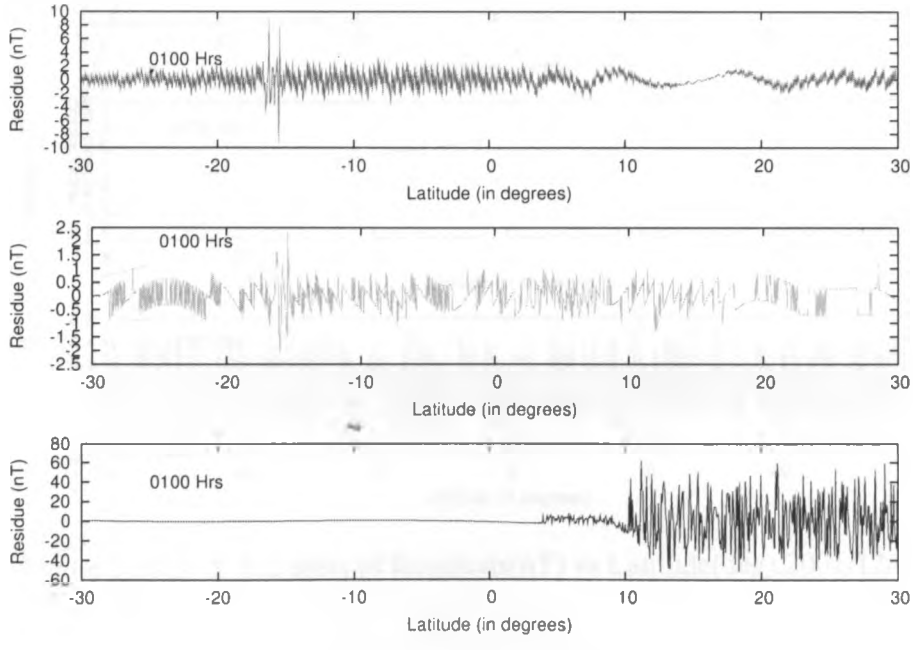

Figure 5.11.1: X,Y,Z plots of Residuals(nT) vs Latitude(deg),2001/12/24

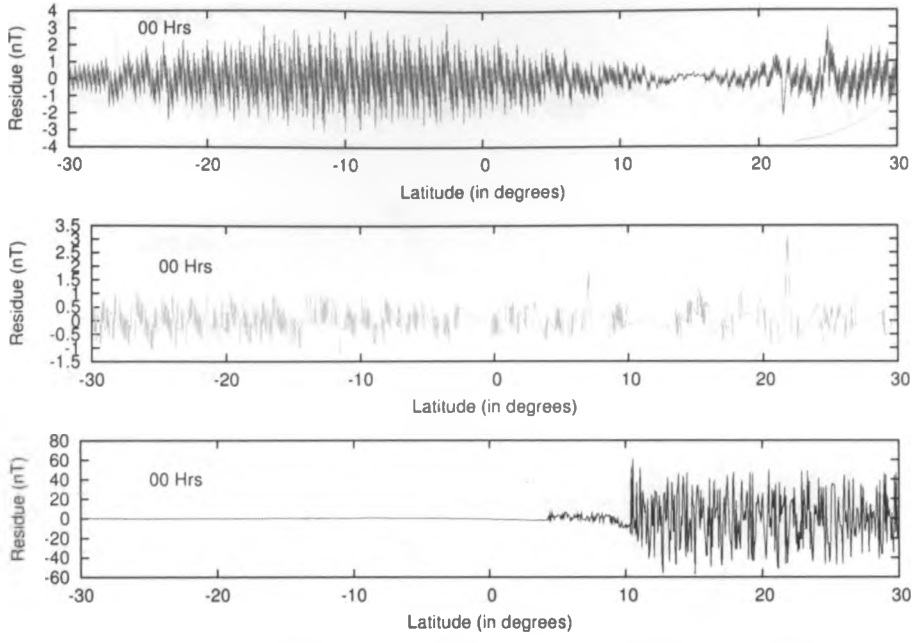

Figure 5.11.2: X,Y,Z plots of Residuals(nT) vs Latitude(deg),2001/12/27

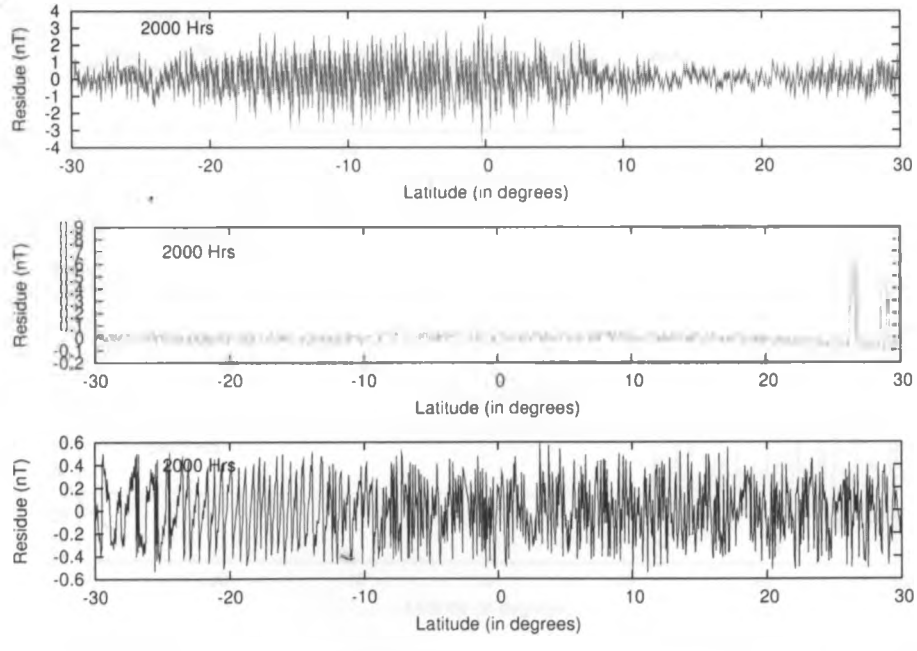

Figure 5.11.3: X,Y,Z plots of Residuals(nT) vs Latitude(deg),2001/12/03

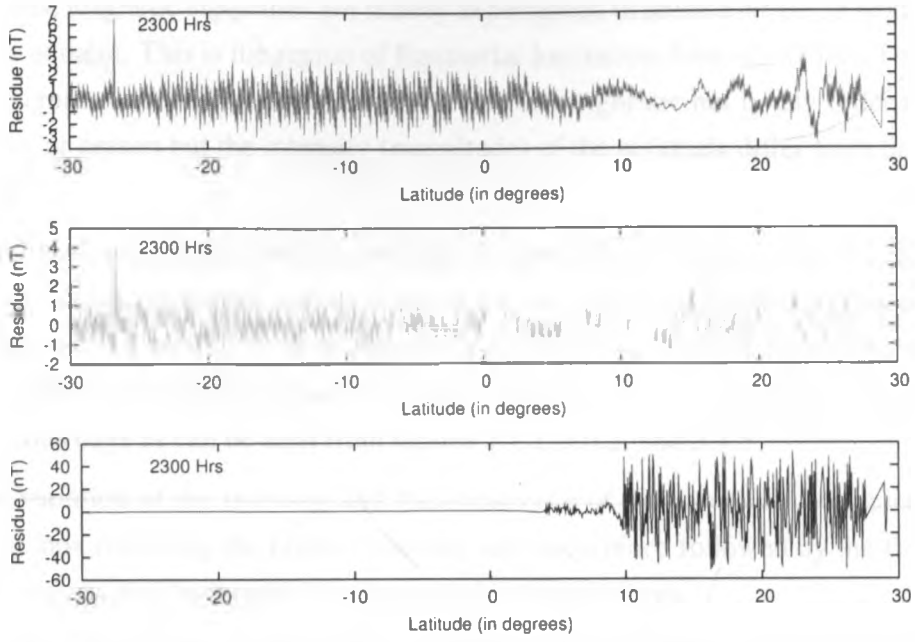

Figure 5.11.4: X,Y,Z plots of Residuals(nT) vs Latitude(deg),2001/12/27

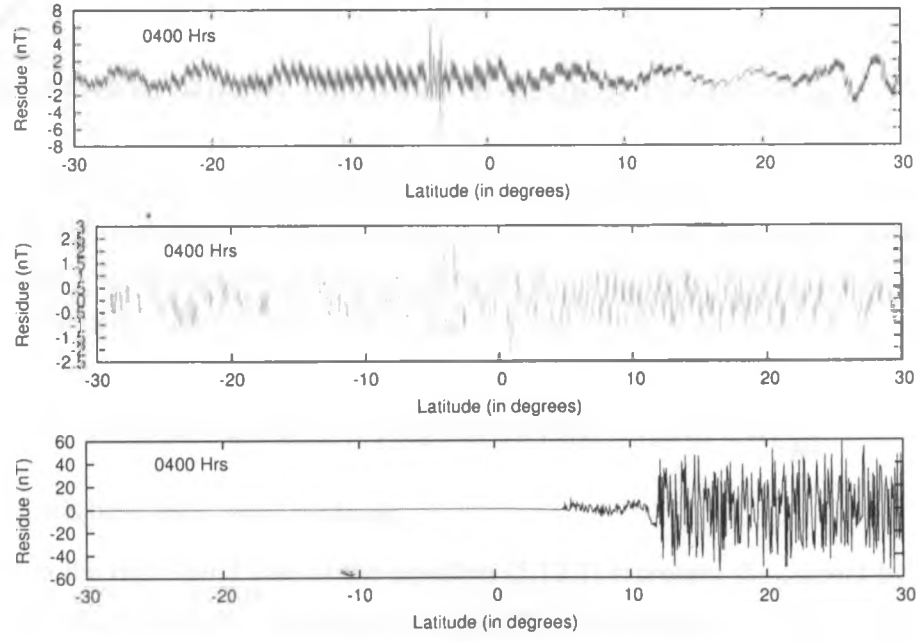

Figure 5.11.5: X,Y,Z plots of Residuals(nT) vs Latitude(deg),2001/12/11

From the data analyzed, we have realized considerable number of very interesting results. In all the figures, we have plotted magnetic field residuals (nT) for all the three magnetic field components against the latitude (degrees).

From our results, magnetic signatures are mainly experienced in latitude of 10-15 degrees on either side of the dip equator. This is the region of Equatorial Ionization Anomaly (EIA). The occurrence of the of the signatures in either pre-midnight or post midnight are not in any order related to the time of the day or season but the intensity (magnitude) of the residuals differ from day to day and season to season.

Even though the y-component of the magnetic field experience the highest occurrence of magnetic signatures, the x-component in all cases, except on 14th November (figure 5.10.2), have the highest intensity. Figures 5.7.2 and 5.7.3 show magnitude of up to 80nT in the x-component. The symmetric occurrence of the signatures on either side of the equator is not quite prevalent but can be noticed in various days as can be seen from figures 5.1.2, 5.6.2, and 5.7.5.

The seasonal variation of the intensity and the occurrence of the signatures is depicted, with the September equinox recording the highest intensity and occurrence followed by the December solstice. March equinox and June solstice experienced little signatures.

The magnetic field signatures, or deflections, or perturbations generally have a positive sign, except in September equinox and December solstice, corresponding to a northward pointing magnetic field.

5.12 Interpretation in terms of F-region currents.

Having detected these unexpected night-time field perturbations, we can now, as stated in our objectives, explain the deflections in the pre-midnight and post-midnight sectors as caused by the F-region currents. To address the possible causes of these currents in the F-region, we invoke equation (2.2.5) with the relevant terms contributing to the current density **J**.

$$\mathbf{J} = \sigma(\mathbf{E} + \mathbf{u} \times \mathbf{B}) + \{N_e m_i \mathbf{g} \times \mathbf{B} - k\nabla[(T_i - T_e)N_e] \times \mathbf{B}\} \frac{1}{B^2} \tag{5.12.1}$$

where all the terms have their usual meaning.

The first term on the right-hand side of the equation (5.12.1) represent the current by the dynamo effect and it is of much particular interest as we can infer the signatures of the $\mathbf{B}_y$ component from it. This component of magnetic field reflects the intensity of the zonal current system caused by the F region dynamo. Considering the F-region as an infinite current sheet, we calculate integrated vertical current density, $\mathbf{J}_z$, (Luhr et al, 2002)

$$\mathbf{J}_z = \frac{1}{\mu_0} \triangle B_y \tag{5.12.2}$$

where **J** is the sheet current density and $\triangle B$ is the magnetic field effect of the current.

The peak-to-peak variation of the magnetic field of B_y component exhibiting a positive to negative transition on the northward passes. The amplitudes are, however, very different. Using equation (5.12.2) we deduce the monthly distribution of the typical current density driven by the F-region dynamo as tabulated below.

month	Jan	Feb	Mar	Apr	May	July	Aug	Sept	Oct	Nov	Dec
current (mA)	0.5	1.6	1.59	1.3	1.59	1.7	5.6	1.59	3.4	7.7	1.8

Figure 5.12.1: Table showing the monthly averaged current densities

The graph showing the monthly averaged current densities is as shown

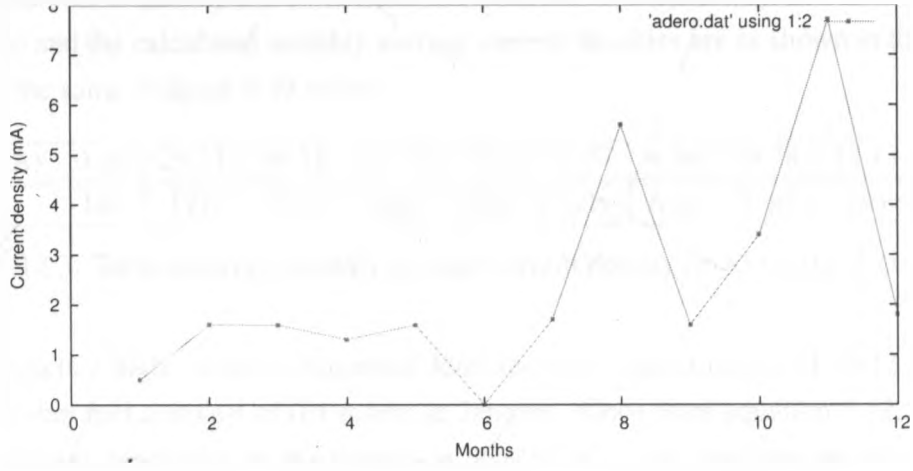

Figure 5.12.2: Monthly average current densities (mA) for Y-component

From the graph, the current density is quite high in the month of November and August.

The dynamo current is expected to get weaker towards midnight due to since the ionospheric conductivity decreases at these times. However our results in August, figure 5.7.2 and November, figure 5.10.3 records some very surprising results. A current density of about 12mA/m and 16mA/m were recorded on 2001 Aug, 08 at 2400LT and 2001 Nov, 14 at 0400LT respectively. This could be attributed to the higher wind velocity.

In the night, as noted earlier, the F-region Pedersen conductivity always dominates over the E-region conductivity in contributing to the total field-line-integrated conductivity, and ion-neutral momentum transfer is confined to the F-region portion of the field line. If the eastward wind varies little along the conducting portion of a field line, then it will generate an electric field of such a magnitude to cause the plasma to drift eastward at a velocity given by equation (2.1.11).

This eastward plasma velocity corresponds to a downward/equatorward electric field that increases in strength toward the east. From our results, the wind direction exhibited both westward and eastward. Its constraints on the electric field prevent it from being large at some apex height, such as an apex height for which the field line descends through a region of relatively large Pedersen conductivity around the latitudes of the equatorial ionization anomaly, then the eastward field at lower heights can become increasingly strong with descending height. This eastward electric field corresponds to upward plasma drifts. Note that although we have estimated the meridional electric field using a two-dimensional geometry, neglecting longitude gradients, it is necessary to con- sider the longitude gradient of the meridional field to understand the origin of the eastward field in this case.

We apply the crude formula (5.12.2) to estimate both the gravity and pressure driven currents. The magnetic signatures of gravity driven currents are believed to be affecting the z-component of the magnetic field and the calculated monthly average current densities are as shown in the figure 5.38 and a plot of the same in figure 5.39 below.

Current (mA)	0.40	29.31	39.78	39.78	37.14	4.77	4.38	39.78	45.13	39.78	39.78
Months	Jan	Feb	Mar	Apr	May	July	Aug	Sept	Oct	Nov	Dec

Figure 5.12.3: Table showing monthly average current density (mA) for the Z-component

The graph depicts a high variation in current densities with highest record of 45.13 mA/m in the month of October and a lowest of 0.4 mA/m in January. Since from equation 5.12.1, the gravity driven currents are dependent on the ionization density, we could attribute the observed current variations to the local plasma density in those months.

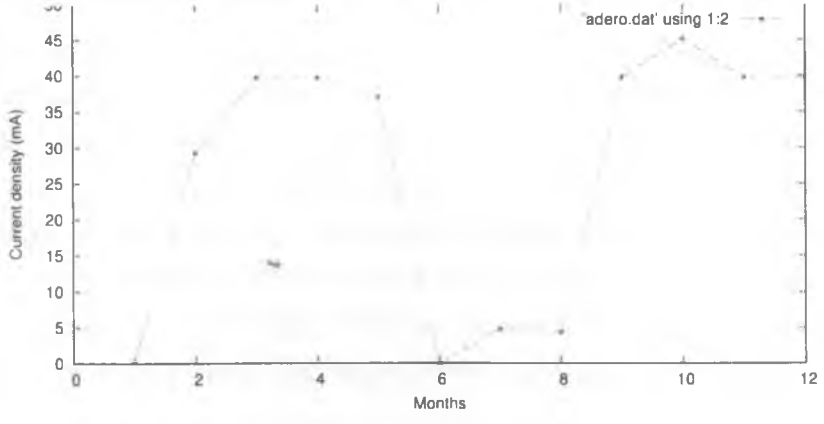

Figure 5.12.4: Monthly averaged current density (mA) for Z-component

The meridional currents (currents on the x-component) were also calculated using the equation

5.12.2 and the monthly averaged values are tabulated in the figure 5.12.5 below. A graph of the same showing monthly variations is plotted in the figure 5.12.6.

Current (mA)	2.39	2.39	3.71	2.12	2.39	2.65	31.35	2.39	2.92	5.84	4.14
Months	Jan	Feb	Mar	Apr	May	July	Aug	Sept	Oct	Nov	Dec

Figure 5.12.5: Table showing the Average current density (mA) per month for X-component

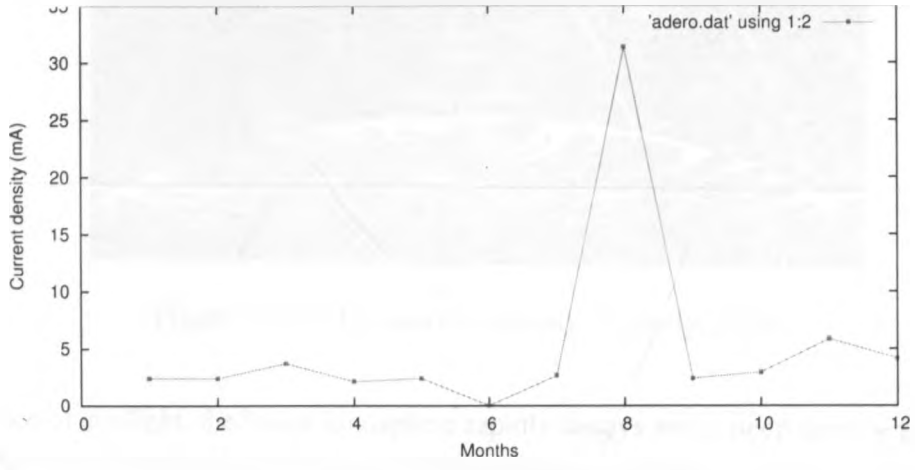

Figure 5.12.6: Monthly average current density (mA) for X-component

The graph depicts a high average current density of 31.35 mA/m in August. Even though we associate the current along this component to be attributed to plasma pressure gradients, the results show that there could be additional contribution from the the dynamo effect. This is so because the currents appear even far past midnight when we don't expect the plasma gradients.

The results in the figures 5.1.1, 5.2.1, 5.2.3, 5.5.1, 5.5.2, 5.5.3, 5.9.1, 5.9.2 and 5.11.3 depicts magnetic field signatures at around 2000hrs and 2200hrs. These reflect currents due to formation of a steep plasma density gradient on the bottom side of the F region, due to recombination of plasma, after sunset which makes the ionosphere unstable to gravitational overturning allowing low-density plasma (plasma bubble) to rise through the ionosphere under the action of the gravitational Rayleigh- Taylor instability. The instabilities are generally referred to as equatorial spread-F (ESF) events and primarily occur at night. The post sunset enhancement of the upward $\mathbf{E} \times \mathbf{B}$ drift raises the F region ionosphere above 300 km as shown in the figure 5.12.7 below.

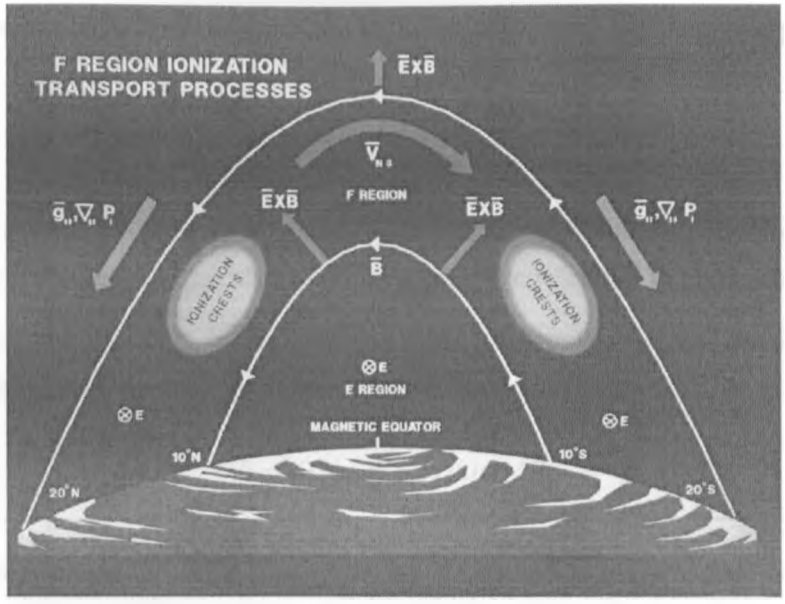

Figure 5.12.7: Equatorial anomaly (Doherty, 2009)

In the absence of sunlight, the lower ionosphere rapidly decays and a steep density gradient develops on the bottomside of the raised F region. This produces one of the conditions for a gravitational Rayleigh-Taylor (R-T) instability to form. A density perturbation on the bottomside can also be significant source. If present, the divergence between the current in the dense F2 region and the depleted region below causes perturbation electric fields to build up. These electric fields cause an upward perturbed $\mathbf{E} \times \mathbf{B}$ drift in the depletions and a downward drift in the enhanced region, which leads to larger perturbations.

The currents inferred from the magnetic signatures in the post mid-night can also be attributed to the drift mechanism illustrated in figure 5.12.7. The currents are triggered by a reversed vertically upward drift, which is initiated by thermospheric neutral wind through F region dynamo. These currents are dominating the area bounded by the Equatorial Ionization Anomaly.

We have inferred the magnetic field residuals seen from 2000hrs to 2200hrs to the plasma driven current. From the equation (2.18), this current is given by

$$\mathbf{J} = -k\nabla\left[(T_i + T_e)\right] N_e / B^2 \tag{5.12.3}$$

This current clearly depends on the temperature difference between the ions and the electrons and is always along the northward (x) component of the magnetic field.

The above equation is employed based on the stationary momentum assumption that every change

in plasma pressure has to be counter-balanced by an adjustment of the magnetic pressure so that

$$\frac{(B+b)^2}{2\mu_0} + \triangle [N_e(T_i + T_e)]k = constant$$

where μ_0 is the susceptibility of free space and b is the magnetic field required to balance the change in plasma pressure. All the other quantities have been defined in equation (2.18).

By neglecting the quadratic term, b^2 because b is much smaller than B and considering stationary, large scale plasma regions we may write the equation above according to Lühr et al. (2003), as

$$b = \triangle N_e(T_i + T_e)k\mu_0 / B$$

Since all the quantities on the right hand side are measured or known, the modification of the magnetic field can be estimated. This so-called diamagnetic effect changes primarily the field strength which can be distinguished reasonably well from the magnetic effects of other current types at low latitudes along the EIA crests.

For typical ionospheric conditions the values of $T_e \approx 2000$K, $T_i \approx 1000$K and $N_e \approx 10^{12} m^{-3}$. At the equator, the ambient field strength is 30,000 nT and inserting the constant $k = 1.38 \times 10^{-23}$, a magnetic field strength (b) of 1.75 nT is obtained.

From our results, the observed magnetic field strengths for the passes between 2000hrs to 2200hrs as in the figures 5.6.1, 5.2.1, 5.2.3, 5.4.2, 5.4.3, 5.5.1, 5.5.2, 5.5.3, 5.6.1, 5.9.2, 5.9.3 and 5.11.3 are tabulated in the table·5.12.8 below

figures from results	5.1	5.3	5.5	5.10	5.11	5.12	5.13	5.14	5.25	5.26	5.27	5.33
magnetic field strength	0.6	0.7	2.5	2.0	2.5	1.5	2.5	2.0	6.0	4.0	4.0	0.8

Figure 5.12.8: x-component magnetic field strengths from 2000hrs-2200hrs

From the table, the average magnetic field strength, b,=2.425nT which is a little higher than the value calculated from the typical ionospheric conditions. This can be explained from the variation of the plasma temperature and density in F-region with time, day and season.

Chapter 6

Conclusion and call for further work

The results from our work has compared favorably with that of First in-situ observation of night-time F region currents with the CHAMP satellite, (Luhr et al, 2002) that is, a spatial confinement of the currents to the near-equatorial region bounded by the Appleton anomaly and their appearance in the pre-midnight and post-midnight sectors.

The current densities are greatly varied along all the three magnetic field components with the z-component recording the highest values. The current densities along y-component is highest in the months of November, about 7.7 mA/m, but generally less than 5.6 mA/m for the rest of the months.

The seasonal variation of the currents is depicted along all the three magnetic field components. The months of September, August and November record the highest current densities with August recording a density of 31.35mA/m along the x-component.

My knowledge about ionospheric currents on the night side and equatorial dynamics has improved significantly. However, the proper description of gravity-driven and pressure-driven currents are still pending, the real possibles causes of the currents as well as the comparison of the magnetic field signatures with the ground-based magnetometers.

It is therefore still a reach area of research that requires intensive study to identify the above short-comings.

Appendix

Appendix A: Storm time Disturbance

The Storm-time Disturbance, D_{st}, index of magnetic storms is derived from low-latitude magnetograms in units of nT and it implies the reduction of the magnetic **H** component of the earth's magnetic field at the equator due to ring currents. It thus serves as a useful indicator of the intensity and duration of individual storm. A typical graph for the disturbance for 08/08/2001 from world data center is as shown,

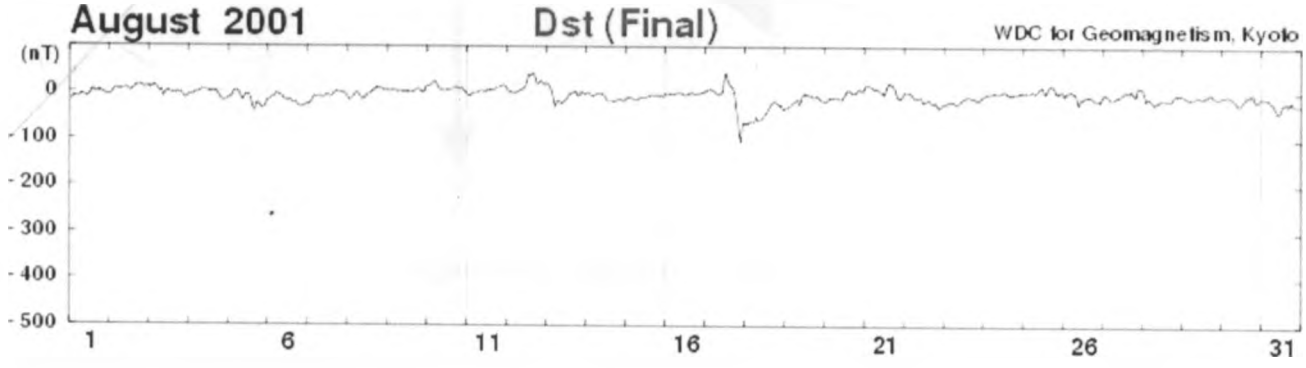

Figure 6.0.1: Dst for 08/08/2001

Appendix B: Geomagnetic field components

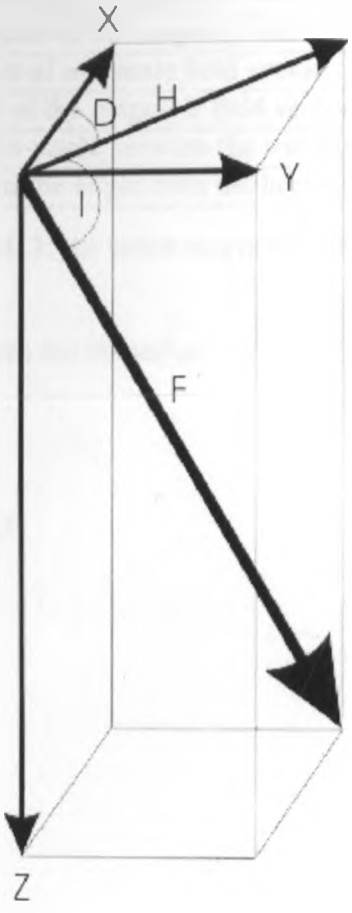

Figure 6.0.2: Magnetic elements

The Earth's magnetic field is a vector quantity; at each point in space it has a strength and a direction. To completely describe it we need three quantities namely:

- three orthogonal strength components (X, Y, and Z);
- the total field strength and two angles (F, D, I);
- two strength components and an angle (H, Z, D)

Component	Description
F	the total intensity of magnetic field vector
H	the horizontal component of magnetic field vector
Z	the vertical component of the magnetic field vector
X	the north component of magnetic field vector
Y	the east component of the magnetic field vector
D	magnetic declination-angle between the true north and the horizontal component of the field.
I	magnetic inclination-the angle from the horizontal plane to the magnetic field vector.

Figure 6.0.3: the seven magnetic components

The seven magnetic field components are related as:

$D = tan^{-1}(\frac{Y}{X})$, $X = Hcos(D)$

$I = tan^{-1}(\frac{Z}{H})$, $Y = Hsin(D)$

$H = \sqrt{X^2 + Y^2}$, $F = \sqrt{X^2 + Y^2 + Z^2}$

Bibliography

1. Dave Anderson and Tim Fuller-Rowell: Space Environment, The Ionosphere, Space Environment Center 325 Broadway, Boulder, CO 80303-3326, 1999.

2. H. Luhr et al: First in-situ observation of night-time F region currents with the CHAMP satellite, GEOPHYSICAL RESEARCH LETTERS, VOL. 29, NO. 10, 10.1029/2001GL013845, 2002.

3. W J G Beynon and P J S Williams: Incoherent scatter of radio waves from the ionosphere, Rep. Prog. Phys., Vol. 41, 1978.

4. Joachim Birn, Richard C. Elphic, William C. Feldman, S. Peter Gary and John T Gosling: Transport Processes in Space Plasmas, 1997.

5. R. A. Heelis: Electrodynamics in the low and middle latitude ionosphere, Journal of Atmospheric and Solar-Terrestrial Physics 66 (2004) 825 – 838.

6. A. L. Aruliah, T.C. Spain, A.D. Aylward, H. Lühr, C.Stolle, M. Förster, P.Ritter: Models and Observations of Ionospheric Conditions, UCL Atmospheric Physics Laboratory, Department of Physics and Astronomy, UK and GFZ Potsdam, Germany .

7. P. C. Brandt, Y. Zheng, and T. S. Sotirelis: The Linkage Between the Ring Current and the Ionosphere System, American Geophysical Union. 10.1029/181GM13, 2008

8. A. J. Ridley, Ann Arbor, A. D. Richmond, T. I. Gombosi, D. L. De Zeeuw, and C. R. Clauer : Ionospheric control of the magnetospheric configuration: Thermospheric neutral winds, Journal of Geophysical Research, Vol. 108, NO. A8, 1328, doi:10.1029/2002JA009464, 2003 .

9. Hermann Lühr, Claudia Stolle, Stefan Maus: Achievements in Characterising Ionospheric and Magnetospheric Fields,2009, London.

10. Stefan Maus, Hermann Lühr, Martin Rother, Kumar Hemant, George Balasis, Patricia Ritter and Claudia Stolle: Fifth generation lithospheric magnetic field model from CHAMP satellite measurements, CIRES, University of Colorado, and NOAA's National Geophysical Data Center, 325 Broadway, Boulder 80305, USA, 2007.

11. C. Stolle , H. Lühr , M. Förster , A. Aylward , T. Spain , A. Aruliah , R. Haagmans , and G. Plank: Swarm Modelling studies of the magnetic effect of low-latitude ionospheric F region currents, Geophysical Research Abstracts, Vol. 11, EGU2009-5291, 2009.

12. J. Park, H. Luhr, C. Stolle , M. Rother, K. W. Min, and I. Michaelis: Field-aligned current associated with low-latitude plasma blobs as observed by the CHAMP satellite, Ann. Geophys., 28, 697–703, 2010.

13. H. S. S. Sinha, S. Raizada: First in situ measurement of electric field fluctuations during strong spread F in the Indian zone, Ann. Geophysicae 18, 523±531 (2000).

14. Endawoke Yizengaw, Mark B. Moldwin, Yogeshwar Sahai, and Rodolfo de Jesus: Strong postmidnight equatorial ionospheric anomaly observations during magnetically quiet periods Journal of Geophysical Research, VOL. 114, A12308, doi:10.1029/2009JA014603, 2009.

15. R Sekar & D Chakrabarty: Equatorial spread-F research in India, a brief review: India Indian Journal of Radio & Space Physics Vol. 37, February 2008.

16. K. Niranjan, P. S. Brahmanandam, P. Ramakrishna Rao, G. Uma, D. S. V. V. D. Prasad, and P. V. S. Rama Rao: Post midnight spread-F occurrence over Waltair during low and ascending phases of solar activity, Ann. Geophys ,2003.

17. Park, H. Luhr, B. G. Fejer, and K. W. Min: Duskside F-region dynamo currents, its relationship with prereversal enhancement of vertical plasma drift, Ann. Geophys., 2010.

18. O. S. Oyekola: A study of evolution/suppression parameters of equatorial post sunset plasma instability, Ann. Geophys., 2009.

19. H. Luhr, S. Maus and M. Rother: Noon-time equatorial electrojet, Its spatial features as determined by the CHAMP satellite JOURNAL OF GEOPHYSICAL RESEARCH, VOL. 109, A01306, doi:10.1029/2002JA009656, 2004.

20. Stefan Maus, Patrick Alken, and Hermann Luhr: Electric fields and zonal winds in the equatorial ionosphere inferred from CHAMP satellite magnetic measurements, GEOPHYSICAL RESEARCH LETTERS, VOL. 34, L23102, doi:10.1029/2007GL030859, 2007.

21. W. G. Baker and D. F. Martyn: Electric Currents in the Ionosphere. I. The Conductivity, Philosophical Transactions of the Royal Society of London. Series A, Mathematical and Physical Sciences, Vol. 246, No. 913, (Dec. 16, 1953).

22. S. Maus, H. Luhr: A gravity-driven electric current in the Earth's ionosphere identified in CHAMP satellite magnetic measurements GEOPHYSICAL RESEARCH LETTERS, VOL. 33, L02812, doi:10.1029/2005GL024436, 2006.

23. J. Hanurnath Sastri, V. K. Meena Varma and S. R. Prabhakaran Nayar: Height gradient of F region vertical drift in the evening equatorial ionosphere, GEOPHYSICAL RESEARCH LETTERS, VOL. 22, NO. 19., 1995.

24. O S Oyekola & Akinremi Ojo and Jolasun Akinrimisi: Nocturnal variations of F-region vertical ionization velocities near the magnetic equator, Indian Journal of Radio & Space Physics Vol. 35, August, 2006.

25. Oyedemi S Oyekola: Seasonal and magnetic activity variations of nighttime ionospheric F-region vertical plasma drifts at Ibadan, Indian Journal of Radio & Space Physics Vol. 36, February 2007.

26. E R de Paula, E A Kherani, M A Abdu, I S Batista, J H A Sobral, I J Kantor, H Takahashi, L F C de Rezende, M T A H Muella, F S Rodrigues, P M Kintner, B M Ledvina, C Mitchell & K M Groves: Characteristics of the ionospheric F-region plasma irregularities over Brazilian longitudinal sector, Indian Journal of Radio & Space Physics Vol. 36, August 2007.

27. Terence J. Sabaka, Nils Olsen and Robert A. Langel: A comprehensive model of the quiet-time, near-Earth magnetic field, Geophys. J. Int. 2002.

28. P. Le Sager and T. S. Huang: Ionospheric currents and field-aligned currents generated by dynamo action in an asymmetric Earth magnetic field, JOURNAL OF GEOPHYSICAL RESEARCH, VOL. 107, NO. A2, 1025, 10.1029/2001JA000211, 2002.

29. J. J. Makela, S. L. Vadas, R. Muryanto, T. Duly and G. Crowley: Periodic spacing between consecutive equatorial plasma bubbles GEOPHYSICAL RESEARCH LETTERS, VOL. 37, L14103, doi:10.1029/2010GL043968, 2010.

30. P.D. Pautet, M. J. Taylor , N. P. Chapagain, H. Takahashi, A. F. Medeiros, F. T. S Sabbas and D. C. Fritts: Simultaneous observations of equatorial F-region plasma depletions over Brazil during the Spread-F Experiment (SpreadFEx), Ann. Geophys., 27, 2371–2381, 2009.

31. The Solar Terrestrial Environment by J. K. Hargreaves.